EBioMedicine xxx (2016) xxx–xxx

Contents lists available at ScienceDirect

EBioMedicine

journal homepage: www.ebiomedicine.com

Research paper

Exogenous Alpha-Synuclein Alters Pre- and Post-Synaptic Activity by Fragmenting Lipid Rafts

Marco Emanuele [a], Alessandro Esposito [a], Serena Camerini [b], Flavia Antonucci [c], Silvia Ferrara [c], Silvia Seghezza [d], Tiziano Catelani [e], Marco Crescenzi [b], Roberto Marotta [e], Claudio Canale [d], Michela Matteoli [f,g], Elisabetta Menna [f,g], Evelina Chieregatti [a,*]

[a] Department of Neuroscience and Brain Technologies, Istituto Italiano di Tecnologia, Genoa, Italy
[b] Department of Cell Biology and Neuroscience, Istituto Superiore di Sanita, Rome, Italy
[c] Department of Medical Biotechnology and Translational Medicine, University of Milan, Milan, Italy
[d] Department of Nanophysics, Istituto Italiano di Tecnologia, Genoa, Italy
[e] Department of Nanochemistry, Istituto Italiano di Tecnologia, Genoa, Italy
[f] CNR Institute of Neuroscience, Milan, Italy
[g] Humanitas Research Hospital, Rozzano, Italy

ARTICLE INFO

Article history:
Received 12 November 2015
Received in revised form 24 February 2016
Accepted 24 March 2016
Available online xxxx

Keywords:
Alpha-synuclein
Lipid rafts
Post-synaptic density
Long term potentiation
Synaptic vesicles' mobilization
Casein kinase 2

ABSTRACT

Alpha-synuclein (αSyn) interferes with multiple steps of synaptic activity at pre-and post-synaptic terminals, however the mechanism/s by which αSyn alters neurotransmitter release and synaptic potentiation is unclear. By atomic force microscopy we show that human αSyn, when incubated with reconstituted membrane bilayer, induces lipid rafts' fragmentation. As a consequence, ion channels and receptors are displaced from lipid rafts with consequent changes in their activity. The enhanced calcium entry leads to acute mobilization of synaptic vesicles, and exhaustion of neurotransmission at later stages. At the post-synaptic terminal, an acute increase in glutamatergic transmission, with increased density of PSD-95 puncta, is followed by disruption of the interaction between N-methyl-D-aspartate receptor (NMDAR) and PSD-95 with ensuing decrease of long term potentiation. While cholesterol loading prevents the acute effect of αSyn at the presynapse; inhibition of casein kinase 2, which appears activated by reduction of cholesterol, restores the correct localization and clustering of NMDARs.

1. Introduction

Alpha-synuclein (αSyn) a small cytosolic protein specifically enriched in the presynaptic nerve terminals (Maroteaux et al., 1988), was found as a major component of intraneuronal inclusion present in the brain of Parkinson's disease (PD) patients (Spillantini et al., 1997). Moreover, multiplication of αSyn gene, and genetic variations in the promoter region leading to increased expression of αSyn, cause familial and sporadic PD (Simon-Sanchez et al., 2009; Singleton et al., 2003). αSyn physiological role is still unclear, but various evidence suggests αSyn involvement in the modulation of distinct steps of the synaptic vesicle (SV) cycle (Lykkebo and Jensen, 2002). αSyn has been considered for long time exclusively an intracellular protein, but its identification in the cerebrospinal fluid and blood plasma (Borghi et al., 2000), suggested a role for extracellular αSyn in the spreading of neurodegeneration (Desplats et al., 2009). Oligomeric and fibrillar αSyn species have been identified as responsible for the toxicity and the spread of disease (Winner et al., 2011), also, a very recent work showed that injection of a non-amyloidogenic, truncated form of αSyn, was able to induce neuronal pathology, pointing to the importance of high dosage of soluble αSyn in the onset of the disease (Sacino et al., 2013). It is now believed that the balance between tetrameric and monomeric forms is important for the correct physiological activity of αSyn (Dettmer et al., 2016).

It is known that αSyn binds phospholipidic membranes, associating with specific microdomains, the lipid rafts (Fortin et al., 2004). At the synapse, receptors and ion channels have a precise localization in the plasma membrane (PM). One of the first proteins that localizes and clusters at synapses during the development is PSD-95, which is lipid raft-anchored (Perez and Bredt, 1998), and functions as multivalent synaptic scaffolding protein. The PDZ domain of PSD-95 was shown to bind the C-terminal tail of N-methyl-D-aspartate receptor (NMDAR) type-2 subunit (NR2b), and this binding is required for the correct localization of the receptor (Kornau et al., 1995).

In the striatum of parkinsonian animals, the localization of NMDAR subunits at synaptic sites is decreased, as is the localization of PSD-95

* Corresponding author at: Department of Neuroscience and Brain Technologies, Istituto Italiano di Tecnologia, Via Morego 30, 16163 Genoa, Italy.
E-mail address: evelina.chieregatti@iit.it (E. Chieregatti).

http://dx.doi.org/10.1016/j.ebiom.2016.03.038

in the synaptic membrane (Nash et al., 2005). NR2b subunits have been found to be specifically reduced in the dopamine denervated striatum of various animal PD models (Gardoni et al., 2006; Hallett et al., 2005). Subunit- and residue-specific phosphorylation differently affects the recruitment of synaptic and extrasynaptic NMDARs (Goebel-Goody et al., 2009). NMDAR binding to PSD95 is decreased by phosphorylation of the NR2b subunit at Serine 1480 (S1480) by casein kinase II (CK2) (Chen and Roche, 2007), as is NR2b surface expression (Chung et al., 2004). In electrophysiological studies, an increased channel gating upon application of purified CK2 has been however observed (Lieberman and Mody, 1999), suggesting a complex and not yet clear regulatory role of CK2. PD progression may also be consequent to molecular defects present at the pre-synaptic site, and indeed alterations in neurotransmitter release, SV trafficking (Murphy et al., 2000), and presynaptic plasticity (Goldberg et al., 2005) are caused by mutation or deletion of various genes involved in PD.

Recently it was demonstrated that application of monomeric extracellular αSyn may perturb calcium homeostasis through alteration of the fluidity of membranes (Melachroinou et al., 2013) or through re-localization of pre-synaptic $Ca_V2.2$ calcium channels in cholesterol-poor areas of the PM (Ronzitti et al., 2014). In rat hippocampal slices exposed to αSyn oligomers, the glutamatergic synaptic transmission was altered with impairment of further potentiation by physiological stimuli (Diogenes et al., 2012). However, the alterations caused by the accumulation of secreted monomeric αSyn, and the mechanisms through which extracellular αSyn contributes to neuronal dysfunction are largely unknown. Here we provide evidence that extracellular monomeric αSyn induces fragmentation of lipid rafts, thus altering raft-partitioning of several membrane-associated proteins. The detachment of proteins from lipid rafts brings about distinct effects in the short and long term exposure to αSyn, increasing basal and evoked calcium entry, neurotransmitter release and post-synaptic activation, and inducing, at later time points, SV exhaustion, defects in the proper clustering of the post-synaptic density (PSD) and impairment of long-term potentiation (LTP). These effects are prevented by cholesterol-loading and CK2 inhibition, respectively.

2. Materials & methods

2.1. Ethics statement

All the experimental procedures followed the guidelines established by the Italian Council on Animal Care and were approved by the Italian Government decree No. 27/2010.

2.2. Reagents

All chemicals, unless otherwise stated were purchased from Sigma-Aldrich (St. Louis, MO). The following primary antibodies were used: anti-PSD95 (Santa Cruz Biotechnology, Dallas, TX, catalog #SC-32290), anti-GAPDH (Santa Cruz Biotechnology, Dallas, TX, catalog #SC-25778) anti-flotillin1 (BD Biosciences, San Jose, CA, catalog #610821), anti-caveolin1 (BD Biosciences, San Jose, CA, catalog #610059), anti-α-synuclein (BD Biosciences, San Jose, CA, catalog #610787), anti-synaptophysin (Synaptic Systems, Goettingen, Germany, catalog #101011), anti-Homer (Synaptic Systems, Goettingen, Germany, catalog #160003), anti-synaptotagmin-1 (Synaptic Systems, Goettingen, Germany, catalog #105011) anti-NMDAR2a (Abcam plc, Cambridge, UK, catalog #ab133265), anti-NMDAR2b (Abcam plc, Cambridge, UK, catalog #ab28373), anti-NMDAR2b phospho S1480 (Abcam plc, Cambridge, UK, catalog #ab73014), anti-PKA (Santa Cruz Biotechnology, #sc-390548), and anti-GluA1 (Abcam plc, Cambridge, UK, catalog #ab32436). Syn peptides (amino acids 12–23 and 34–45) were obtained from Primmbiotech.

2.3. Expression plasmids

GFP-E-Syt1 was a kind gift from Pietro De Camilli (Yale School of Medicine, New Haven, CT). VAMP2-GFP was a kind gift from Flavia Valtorta (San Raffaele Scientific Institute, Milan, Italy). PSD-95-RFP was a gift from Johannes Hell (Addgene, Cambridge, MA, plasmid #52671).

αSynS129E-GFP was generated from αSyn-GFP (a gift from David Rubinsztein, Addgene, Cambridge, MA, plasmid #40822) with GeneArt™ Site-Directed Mutagenesis System (Life Technologies, Paisley, UK).

2.4. Neuronal culture

Primary cultures were obtained from hippocampi or cortices of C57BL6J mice (Harlan Laboratories Inc., Indianapolis, IN, USA) at embryonic day 18 (E18). Embryos were removed and dissected under sterile conditions. Cortices and hippocampi were dissociated by enzymatic digestion in 0.125% trypsin-EDTA (Life Technologies, Paisley, UK) for 30 min at 37 °C and 0.25 mg/ml DNase in Hank's Balanced Saline Solution (Life Technologies), 2 mM calcium chloride (Sigma-Aldrich, St. Louis, MO, USA) for 30 min at 37 °C. Trypsin activity was blocked by adding complete medium which consists of Neurobasal Media (Life Technologies) supplemented with 2% B27 (Life Technologies), 2 mM GlutaMax (Life Technologies), 100 U/ml penicillin-streptomycin (Life Technologies), and 10% fetal bovine serum (Life Technologies). After trypsinization, hippocampi and cortices were rinsed in complete medium without FBS, dissociated with a plastic pipette, and 20,000–40,000 hippocampal or cortical neurons were plated at a concentration of $0.20–1 \times 10^5$ cells/ml onto 18 mm or 25 mm diameter coverslips pre-coated with 0.1 mg/ml poly-D-lysine.

For LTP experiments primary cultures were obtained from hippocampi of E18 Sprague Dawley rats (Charles River). Dissociated cells were plated onto coverslips coated with poly-L-lysine at a density of 400 cells/mm^2. The cells were maintained in Neurobasal (Invitrogen, San Diego, CA) with B27 supplement and antibiotics, 2 mM glutamine, and 10 mM glutamate.

2.5. Electroporation and transfection of primary hippocampal and cortical neurons

For experiments with VAMP2 and E-Syt1, neurons (1×10^6) were electroporated with 1 μg of DNA using P3 Primary Cell 4D-Nucleofector Kit and the pulse code CU133 on the 4D-Nucleofector System (Lonza Group Ltd., Basel, Switzerland). For experiments with PSD-95, neurons were transfected using Lipofectamine 2000 (Life Technologies) at DIV 17–18. Cultures were analyzed at DIV 20–21.

2.6. Brain slices preparation

20-day old mice (C57BL/6JRccHsd or C57BL/6S, Harlan, Udine, Italy) were anesthetized with isofluorane and decapitated. Brains in cold carboxygenated artificial cerebrospinal fluid (ACSF, 124 mM NaCl, 3 mM KCl, 2 mM $CaCl_2$, 25 mM $NaHCO_3$, 1.1 mM $NaH2PO_4$, 2 mM $MgSO_4$, and 10 mM D-glucose), equilibrated with 95% O_2 and 5% CO_2 to yield pH 7.4, were sectioned on a vibrating microtome at a thickness of 100–300 μm.

2.7. αSyn purification

The construct encoding the full-length human wild-type αSyn inserted in the pET21d plasmid was a kind gift from Brett Lauring (Columbia University, New York, NY). Purification was performed as described previously (Martinez et al., 2003). Bacteria were induced during the exponential phase with 1 mM isopropyl β-D-1-thiogalactopyranoside for 2 h and harvested by centrifugation. The pellet was solubilized in 20 mM HEPES/KOH, pH 7.2, and 100 mM KCl (buffer A) and heated

Please cite this article as: Emanuele, M., et al., Exogenous Alpha-Synuclein Alters Pre- and Post-Synaptic Activity by Fragmenting Lipid Rafts, EBioMedicine (2016), http://dx.doi.org/10.1016/j.ebiom.2016.03.038

for 5 min at 90 °C. The cell lysate was centrifuged at 72,000 × *g* for 30 min, and the supernatant was loaded on a HiTrap monoQ column (GE Healthcare). αSyn was eluted with a liner gradient of KCl from 100 to 500 mM, and the fractions of interest were concentrated using a Centricon centrifugal filter (Millipore) before loading on a Superose 12 column in buffer A (GE Healthcare). The fractions containing αSyn were pooled, concentrated, and stored at −80 °C. To control αSyn purity, 1 mg of purified Syn was loaded on top of a Superdex 75 10/300 column (GE Healthcare) and eluted at 0.5 ml/min on an AKTA Purifier apparatus. Optical density (OD) was continuously measured at 280 nm. Control samples were incubated with the elution buffer used for αSyn purification.

2.8. Lipid raft isolation

All procedures were performed at 4 °C. Lipid raft isolation was performed on cortico-striatal brain slices as described previously (Butchbach et al., 2004). Slices were lysed and the extracts were incubated for 1 h at 4 °C with 170 μl/slice of PBS containing 1% of Triton X-100 and Complete Mini protease inhibitor (Roche Basel, Switzerland). The total protein concentration was measured with the BCA assay kit (Life Technologies). For each sample, the same amount of proteins was added with sucrose to obtain a 40% final concentration. 900 μl of the extract was placed on the bottom of an ultracentrifugation tube and a discontinuous 5–30% sucrose gradient was formed on top of the extract. The gradient was then centrifuged at 47,000 rpm for 16 h at 4 °C in a MLS 50 rotor (Beckman Coulter). 500 μl fractions were collected from the top of each gradient (Beckman Coulter); rafts were recovered between 2 and 3 ml from the top of the gradient. 5× SDS-PAGE loading buffer (100 mM Tris, pH 7.5, 7.5 mM EDTA, 10% SDS, 10% β-mercaptoethanol, 50% glycerol, and 0.02% bromophenol blue) was added to the fractions.

2.9. Sample purification and protein identification by mass spectrometry analysis

Raft fractions collected from the gradient were separated on a 1D-gel NuPAGE 4–12% (Novex, Invitrogen) run in morpholinepropanesulfonic acid (MOPS) buffer and stained with the Colloidal Blue Staining kit (Invitrogen). Whole gel lanes from both control samples and samples incubated with αSyn were cut into 10 sequential slices. Each band was subjected to cysteine reduction by DTT and alkylation by iodoacetamide, and finally digested with trypsin. Peptide mixtures were analyzed by nanoflow reversed-phase liquid chromatography tandem mass spectrometry using an HPLC Ultimate 3000 (DIONEX) connected on line with a linear Ion Trap (LTQ, Thermo Electron). After desalting in a trap column (Acclaim PepMap 100 C18, DIONEX), the peptides were separated in 10 cm long silica capillary (Silica Tips FS 360-75-8, New Objective), packed in-house with 5 μm, 200 Å pore size C18 resin (Michrom BioResources). Peptides elution was obtained with a 40 min linear gradient from 5% to 60% acetonitrile in the presence of 0.1% formic acid. Analyses were performed in positive ion mode (1.7–1.8 kV HV) and a data dependent mode acquisition allowed the fragmentation of the five most abundant ions. Tandem mass spectra were searched against Swiss-Prot database containing mouse proteins through SEQUEST algorithm incorporated in Bioworks software (version 3.3, Thermo Electron). Searches took in account specific trypsin hydrolysis, with one possible miss cleavage. Proteins were identified with at least two peptides, cross-correlation scores of 1.8, 2.5, and 3 respectively for one, two, and three charged peptides and a probability cut-off for randomized identification of $p < 0.001$.

2.10. Co-immunoprecipitation

Proteins from brain slices were extracted with 1% Triton in PBS, and protease inhibitors (Roche, Basel, Switzerland). For immunoprecipitation assays, 200 μg of total extract were incubated overnight at 4 °C with 1 μg of antibody per 100 μg of total protein, and 50 μl protein G agarose beads (Pierce, Life Technologies). Beads were washed four times with 1% Triton in PBS. Immunoprecipitates and 1/10 of total extracts were resolved by reducing SDS-PAGE.

2.11. Immunoblot analysis

SDS-PAGE and electrotransfer of membranes were performed as described previously (Laemmli, 1970). Immunoreactive bands were detected by chemiluminescence, and images were acquired using an LAS AF 4000 apparatus (GE Healthcare). Band intensities were measured by Image Quant analysis software (GE Healthcare).

2.12. Immunocytochemistry and confocal microscopy

Transfected primary cortical neurons cultured on coverslips were fixed in 4% paraformaldehyde/30% glycerol in PBS for 5 min. The coverslips were washed in PBS four times and were incubated with primary antibodies in blocking buffer (0.5% Triton X-100, 5% goat serum). After four washes in PBS, neurons were incubated with fluorescently-conjugated secondary antibodies in blocking buffer. The coverslips were washed in PBS four times and dipped in distilled water before being mounted in ProLong Gold Antifade Reagent (Life Technologies). Capture of confocal images was performed using a laser scanning confocal microscope (SP5 Upright, Leica) with a 63X oil-immersion objective. Each image consisted of a stack of images taken through the z-plane of the cell. Confocal microscope settings were kept the same for all scans in each experiment. Number of PSD-95 puncta and the length of dendrites were measured using the open access ImageJ software (http://imagej.nih.gov/ij/). Brain slices were fixed with 4% PFA in PBS, permeabilized and incubated for 1 h at room temperature in blocking buffer. The slices were then incubated overnight with primary antibodies in a goat serum solution (5% goat serum, 0.3% Triton X-100, NaN_3 0.02%). After 3 washes, slice were incubated for 2 h at room temperature with fluorochrome coupled secondary antibodies and mounted with ProLong Gold mounting medium. Samples without primary antibody were used as negative control. Capture of confocal images was performed using a laser scanning confocal microscope (SP5 Upright, Leica) with a 63X oil-immersion objective. Image acquisition settings were determined using two random control slices so as to obtain visible signal without saturation. Excitation and detection parameters were subsequently kept constant for all slices. Co-localization analysis was performed using ImageJ software and the JACoP plug-in.

2.13. Analysis of spines' number and size

Brain slices of 200 μm thickness were lightly fixed with 1.5% PFA in PBS. Solid DiI crystals (1,1′-dioctadecyl-3,3,3′,3′-tetramethylindocarbocyanine perchlorate) were applied to the slices under a dissecting microscope. Slices were incubated in PBS at room temperature for 1 h to allow DiI crystals to diffuse fully along the neuronal membranes. Slices were then fixed again with 4% PFA for 30 min, washed 3 times with PBS mounted with ProLong Gold mounting medium. Capture of confocal images was performed using a laser scanning confocal microscope (SP5 Upright, Leica) with a 63X oil-immersion objective. Each image consisted of a stack of images taken through the z-plane of the cell. Confocal microscope settings were kept constant for all scans in each experiment. Number and size of spines and the length of dendrites were measured using the open access ImageJ software (http://imagej.nih.gov/ij/).

2.14. Cell culture electrophysiology

Whole-cell patch-clamp recordings of mEPSCs were obtained from 14–16 DIV neurons using a Multiclamp 700A amplifier

Please cite this article as: Emanuele, M., et al., Exogenous Alpha-Synuclein Alters Pre- and Post-Synaptic Activity by Fragmenting Lipid Rafts, EBioMedicine (2016), http://dx.doi.org/10.1016/j.ebiom.2016.03.038

(Molecular Devices) and pClamp-10 software (Axon Instruments, Foster City, CA). Recordings were performed in the voltage-clamp mode. Currents were sampled at 10 kHz and filtered at 2–5 kHz. External solution [Krebs Ringer's-HEPES (KRH)] had the following composition (in mM): 125 NaCl, 5 KCl, 1.2 $MgSO_4$, 1.2 KH_2PO_4, 2 $CaCl_2$, 6 glucose, 25 HEPES-NaOH, and pH 7.4. Cells were voltage-clamped at a holding potential of −70 mV to selectively identify AMPA-mediated postsynaptic currents. Recordings of mEPSCs were obtained in the presence of Tetrodotoxin (TTX, 1 μM, Tocris, Bristol, UK) to block spontaneous action potentials' propagation. Recording pipettes, tip resistances of 3–5 MΩ, were filled with the intracellular solution of the following composition (in mM): 130 potassium gluconate, 10 KCl, 1 EGTA, 10 HEPES, 2 $MgCl_2$, 4 MgATP, and 0.3 Tris-GTP. Off-line analysis of miniature events was performed by the use of Clampfit-pClamp-10 software and events had to exceed a threshold of 10 pA to be taken into account.

For chemical LTP experiments, recordings of mEPSCs were performed using the same intracellular solution of miniature events while glycine (100 μM, Sigma-Aldrich, Milan, Italy) was applied for 3 min at room temperature in Mg^{2+}-free KRH also containing TTX (0.5 μM), bicuculline (20 μM, Tocris, Bristol, UK) and strychnine (1 μM, Sigma-Aldrich, Milan, Italy).

2.15. Supported lipid bilayers' preparation and AFM measurements

Supported lipid bilayers (SLBs) were obtained by fusion of large unilamellar vesicles (LUVs) on freshly cleaved mica. Lipids used for vesicle preparation were: 1,2-dioleoyl-*sn*-glycero-3-phosphocholine (DOPC), sphingomyelin (SM) (brain, porcine), ganglioside GM1 (brain, ovine), all purchased from Avanti Polar Lipids (Alabaster, AL, USA), and cholesterol (chol), from Sigma-Aldrich. Lipid powders were dissolved in chloroform/methanol 2:1 and mixed according to the chosen composition: DOPC/SM 2:1 (mol/mol) + 1% mol chol + 5% mol GM1. Aliquots containing 0.5 mg of lipids were then incubated overnight under vacuum, in order to remove any solvent trace, and resuspended in Milli-Q water (Millipore, resistivity 18.2 MΩ·cm) at a concentration of 0.5 mg/ml, in order to form multilamellar vesicles (MLVs). MLV suspension was sonicated at 60 °C for 1 h and successively extruded 11 times using a commercial extruder (Avanti Polar Lipids) through a polycarbonate membrane with pore size of 100 nm to produce LUVs. Extrusion was performed on a hot plate, which was kept at 60 °C. After cooling at room temperature, LUV suspension was diluted 5 fold with Milli-Q water and mixed with 1 μM αSyn. After 30 min incubation, LUVs with α-Syn were administered to freshly cleaved mica attached to a microscope slide. Right after, 2 mM $CaCl_2$ was added in order to trigger vesicle fusion. Samples were then stored at 60 °C in a humid, closed chamber for 15 min, and successively incubated at room temperature for 2 h. Before AFM investigation, samples were carefully rinsed with Milli-Q water, in order to remove vesicle excess from the liquid phase. Control samples were prepared following the same protocol, using a LUV suspension without αSyn.

AFM measurements were performed using a Nanowizard III atomic force microscope (JPK Instruments, Germany) mounted on an Axio Observer D1 inverted optical microscope (Carl Zeiss, Germany). Quantitative Imaging (QI) Advanced software module was included in the setup. V-Shaped DNP silicon nitride cantilevers (Bruker, Billerica, MA), with a nominal spring constant ranging from 0.12 to 0.48 N/m, a resonance frequency in air ranging from 40 to 75 kHz, and a tip with typical curvature radius of 20–60 nm were used. The actual spring constant of each cantilever was determined in situ, using the thermal noise method. Images of SLBs were acquired in liquid, using QI mode; QI images were produced through the collection of 256 × 256 force-distance curves, with maximum force load as close as possible to the contact point, typically 0.8 nN. Tip vertical speed during curve acquisition was 30 μm/s.

2.16. TIRF live-imaging

Time-lapse images of mouse cortical neurons electroporated with VAMP2-GFP or E-Syt1-GFP were taken in TIRF mode set at 100 nm on Leica TCS SP5 microscope with a 100× objective (Leica Microsystems, Wetzlar, Germany) at 1 frame per min for 60 min. For the analysis of evoked fusion coverslips were mounted in an open quick change chamber with stimulation electrodes (Warner Instruments, Hamden, CT) and were stimulated with 100 APs at 20 Hz. The images were acquired with 2 × 2 binning to avoid the photobleaching and with an exposure time of 50 ms.

2.17. Electron microscopy

Cortico-striatal slices (100 μm) were washed in cold PBS, collected in the same buffer and fixed for 1 h in 2% glutaraldehyde and 2% paraformaldehyde in 0.1 M cacodylate buffer. After fixation, slices were processed by high pressure freezing and freeze substitution. Disks of tissue (1.2 mm in diameter) corresponding to the dorsal portion of the striatum were high-pressure frozen (Leica EM PACT2), freeze substituted (Leica EM AFS2) in acetone containing 0.1% tannic acid, 0.5% uranyl acetate in 2% OsO4 and embedded in SPURR resin (modified from Rostaing 2004). Sections of about 70 nm were cut with a diamond knife (DIATOME) on a Leica EM UC6 ultramicrotome, and stained with lead citrate and uranyl acetate. TEM images were collected using a FEI Tecnai F20 equipped with a field-emission gun (FEG) and recorded with a 2 k × 2 k Mp Gatan BM UltraScan Charge-Coupled Device (CCD) camera.

2.18. Statistical analysis

Two-tailed tests were performed using Prism 5 (GraphPad Software, Inc.) for comparison of two groups and expressed as mean values ± standard error of means (SEM). For all pair wise multiple comparison procedure, Holm–Sidak method was used for one-way analysis of variance (ANOVA) using Prism 5 (GraphPad Software, Inc.), and the data were expressed as mean values ± SEM. P-values less than 0.05 were considered to be statistically significant.

3. Results

3.1. Extracellular αSyn affects raft-partitioning of several proteins inducing lipid raft fragmentation

We previously showed that, in neurons incubated with αSyn, $Ca_v2.2$ calcium channels shifted from raft domains to cholesterol-poor areas of the PM, becoming concomitantly active (Ronzitti et al., 2014). To verify if re-localization of proteins could be a generalized phenomenon involving also other plasma membrane proteins, we performed proteomic analysis of raft fractions separated on a sucrose density gradient loaded with lysates from slices treated or not with αSyn. After treatment with αSyn fewer proteins were found in raft fractions, i.e. ~12% less than in control sample (Fig. 1a). We found that ~25% of the proteins that completely disappeared from lipid rafts upon incubation with αSyn were transmembrane and PM associated pre- and post-synaptic proteins (Fig. 1b), such as channels, receptors, proteins belonging to the active zone or the PSD, and cytoskeleton-related proteins (Fig. 1c). The changes induced by extracellular αSyn on raft partitioning of several PM proteins were suggestive of an alteration of the structure or number of raft microdomains. We therefore investigated by atomic force microscopy (AFM) the effect of αSyn on lipid bilayers supported on mica substrates. Model membranes consisted of monounsaturated phospholipids and sphingomyelin, cholesterol and ganglioside GM1 with or without αSyn. The lipids within this mixture segregate in areas with distinct degrees of order resembling the organization of the cellular membranes. In particular, GM1, sphingomyelin and most of cholesterol form the lipid ordered phase, considered as raft-like domain. The two domains are easily recognizable in AFM since ordered domains were 1.8 ± 0.1 nm thicker than disordered

Please cite this article as: Emanuele, M., et al., Exogenous Alpha-Synuclein Alters Pre- and Post-Synaptic Activity by Fragmenting Lipid Rafts, EBioMedicine (2016), http://dx.doi.org/10.1016/j.ebiom.2016.03.038

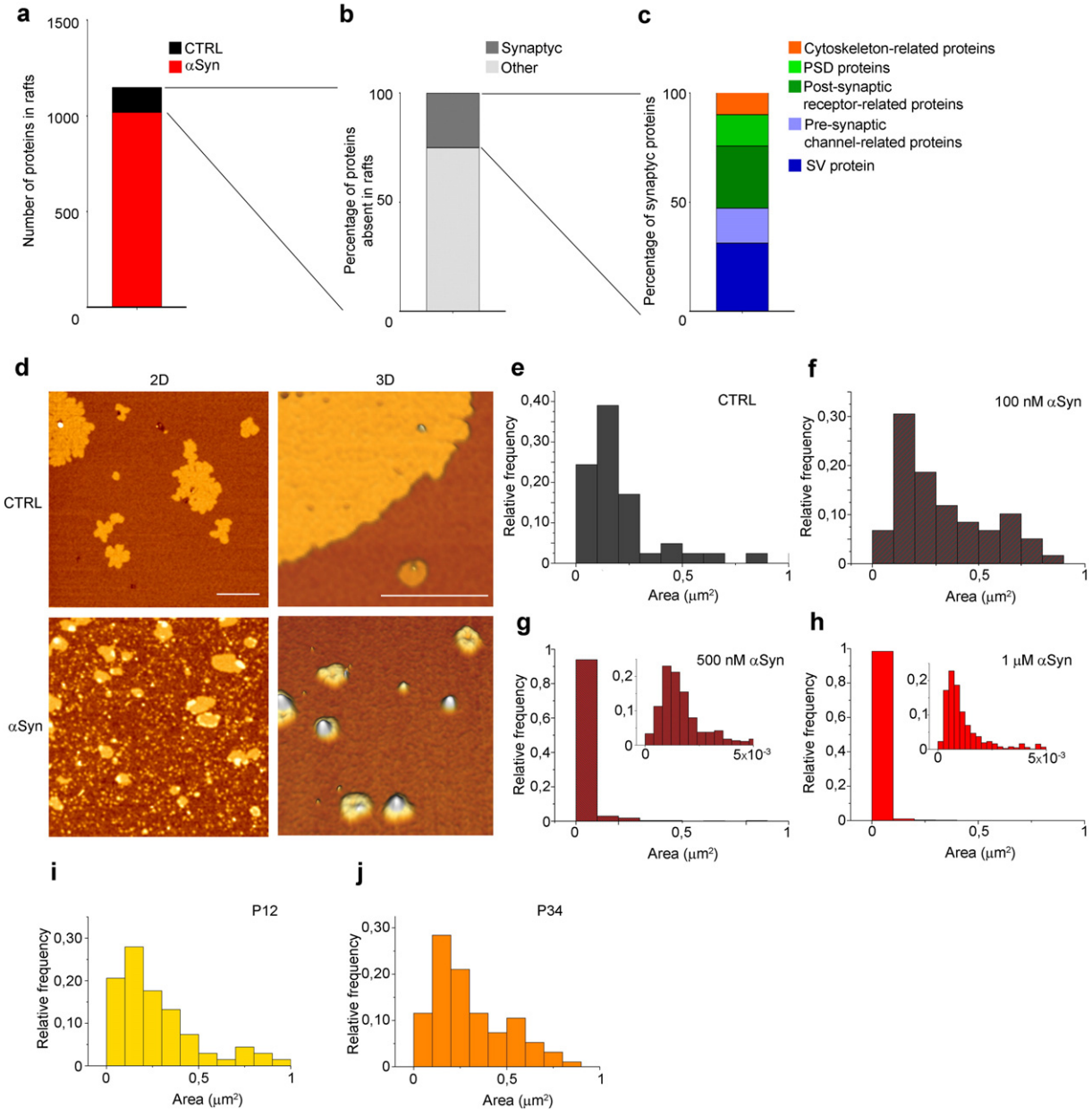

Fig. 1. αSyn alters raft-partitioning of proteins and induces fragmentation of lipid rafts. (a) Histogram showing the total number of proteins found in raft fractions (1048 proteins) in the control sample (CTRL), and the number of proteins missing in the sample treated with αSyn (132 proteins). n = 4. (b) Histogram showing the percentage of synaptic proteins (25%) on the total number of proteins missing in lipid rafts upon incubation with αSyn. (c) Histogram showing the percentage of SV associated proteins (31.2%), pre-synaptic channel-related protein (16%), post-synaptic receptor-related proteins (28.5%), PSD-related protein (14.3%) and cytoskeleton-related proteins (9.9%) on the total number of synaptic proteins missing in rafts in the sample treated with αSyn. (d) Representative bidimensional (left panels, scale bar: 1 μm) or tridimensional (right panels, scale bar: 0.5 μm) images of reconstituted membrane bilayer in the presence or not of 1 μM αSyn. (e) Distribution of the area of raft domains in control bilayers. n = 12 5 × 5 μm^2 images from 5 independent experiments. (f) Distribution of the area of raft domains in bilayers containing 100 nM αSyn. n = 8 5 × 5 μm^2 images from 3 independent experiments. (g) Distribution of the area of raft domains in bilayers containing 500 nM αSyn; in the inset is shown the distribution of raft areas between 0 and 5 × 10^{-3} μm^2, populated by extremely small lipid raft domains that characterize the sample incubated with αSyn. n = 12 5 × 5 μm^2 images from 5 independent experiments. (h) Distribution of the area of raft domains in bilayers containing 1 μM αSyn. n = 15 5 × 5 μm2 images from 6 independent experiments. (i) Distribution of the area of raft domains in bilayers containing 1 μM P12. n = 13 5 × 5 μm^2 images from 6 independent experiments. (j) Distribution of the area of raft domains in bilayers containing 1 μM P34. n = 12 5 × 5 μm^2 images from 4 independent experiments.

ones. The structure of raft-like domains appeared dramatically changed in the presence of αSyn, as shown by bidimensional and tridimensional (Fig. 1d) AFM topography. While in control bilayers the size of rafts' microdomains was ranging from 0 to 1 μm^2 (Fig. 1e), αSyn in a concentration starting from 500 nM to 1 μM induced fragmentation of rafts with the majority of them falling in the range between 0 and 5 × 10^{-3} μm^2 (Fig. 1g and h). 100 nM αSyn, the lowest concentration applied, failed to produce any significant effect compared to controls (Fig. 1f). To exclude the possibility that the effect of αSyn could be unspecific, we employed two αSyn peptides: P34 (aa 34-45), i.e. the glycosphingolipid-binding domain of Syn, and P12 (aa 12-23), a peptide with no recognized function, as a control. None of these peptides determined measurable effects on lipid rafts' size (Fig. 1i and j), indicating that the whole protein is required for its activity.

3.2. Extracellular αSyn affects the localization and the interaction of PSD-95 and NR2b

Based on the results obtained with proteomic experiments, that highlighted a wide-ranging effect of αSyn on the re-localization of

Please cite this article as: Emanuele, M., et al., Exogenous Alpha-Synuclein Alters Pre- and Post-Synaptic Activity by Fragmenting Lipid Rafts, EBioMedicine (2016), http://dx.doi.org/10.1016/j.ebiom.2016.03.038

multiple proteins, we hypothesized that repartitioning of post-synaptic proteins could contribute to the described αSyn-driven defects in post-synaptic activity. To investigate the possible alteration of post-synaptic proteins localization upon exposure to αSyn, cortico-striatal brain slices were incubated with or without αSyn for 2 h, homogenized, and the extracts were loaded at the bottom of a sucrose gradient. Flotillin-1 was

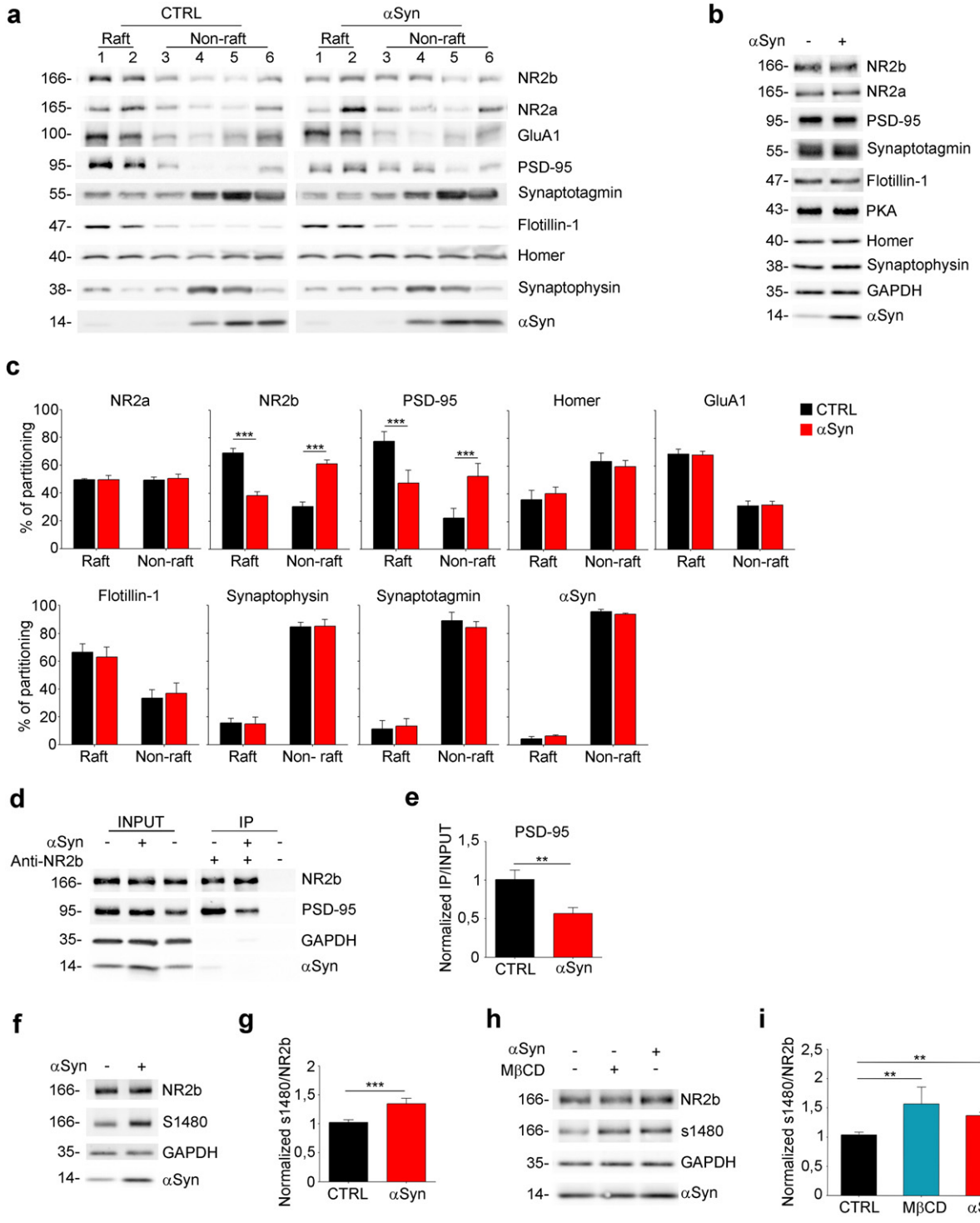

Fig. 2. Extracellular αSyn affects the localization and the interaction of PSD-95 and NR2b. (a) Immunoblot of fractions collected from sucrose gradients loaded with extracts from cortico-striatal brain slices incubated without (CTRL) or 5 μM αSyn. It is shown the distribution of proteins in raft (fractions 1 and 2) and non-raft (fractions 3–6) domains. Overlay was performed with the antibodies indicated on the right. (b) Immunoblot showing the total level of proteins in samples incubated or not with 5 μM αSyn. (c) Quantitative evaluation by densitometry of the protein content in raft or non-raft fractions expressed as percentage of the total protein amount calculated by the sum of the amount of the protein of interest in each fraction. n = 5. (d) Immunoblot showing co-immunoprecipitation with anti-NR2b antibody from cortico-striatal brain slices incubated or not with 5 μM αSyn. The three left lanes show extracts (INPUT: 10% of the total). The three right lanes show immunoprecipitates (IP). (e) Quantitative evaluation by densitometry of co-immunoprecipitated PSD-95 band normalized on the INPUT. n = 3. (f) Immunoblot showing S1480 phosphorylation level in samples derived from brain slices incubated or not with 5 μM αSyn. (g) Quantitative evaluation by densitometry of S1480 phosphorylation level normalized on NR2b level. n = 5. (h) Immunoblot showing S1480 phosphorylation level in samples from brain slices incubated with 0.1 mg/ml MβCD or with 5 μM αSyn. (i) Quantification by densitometry of S1480 phosphorylation level normalized on NR2b. n = 3. Data are expressed as mean ± SEM (c, e, g, i). Statistical significance determined by 2way-ANOVA (c), by t-test (e, g), or 1way-ANOVA (i). **p < 0.01, ***p < 0,001.

Please cite this article as: Emanuele, M., et al., Exogenous Alpha-Synuclein Alters Pre- and Post-Synaptic Activity by Fragmenting Lipid Rafts, EBioMedicine (2016), http://dx.doi.org/10.1016/j.ebiom.2016.03.038

used as a marker for lipid rafts (Bickel et al., 1997), and was mostly recovered in raft fractions (1–2), whereas proteins not associated with lipid rafts, such as synaptotagmin-1 or synaptophysin, were enriched at the bottom of the gradient (fractions 3–6). The NR2b subunit of NMDAR and PSD-95, which in control conditions were recovered in fractions 1 and 2, shifted into heavier fractions upon addition of αSyn to slices (Fig. 2a). αSyn did not impact the total amount of proteins, as shown by quantitative western blotting (Fig. 2b). The quantitative evaluation of the protein bands in the distinct fractions indicated that in control sample ~78% of PSD-95 and ~70% of NR2b were localized in lipid rafts, while only ~50% of PSD-95 and ~40% of NR2b were found in raft fractions after incubation with αSyn (Fig. 2c). Other proteins, such as NR2a, the GluA1 subunit of the α-amino-3-hydroxy-5-methyl-4-isoxazolepropionic acid (AMPA) receptor, Homer, synaptotagmin-1 and synaptophysin were not affected by αSyn (Fig. 2a–c). The two αSyn soluble peptides did not alter the localization of NR2b and PSD-95 in lipid rafts (Supplementary Fig. 1a and b). Taken together, these results indicate a specific effect of αSyn on raft-partitioning of multiple proteins. It has been shown an effect of extracellular αSyn that, by a prion-like mechanism, affects the oligomerization state of the endogenous protein (Volpicelli-Daley et al., 2011). To exclude the possibility of the involvement of intracellular mouse αSyn in the PM disorganization and consequent altered raft-partitioning of PM-associated proteins, we performed lipid raft isolation from slices derived from a αSyn knocked out mouse. As for the wt mouse, NR2b and PSD-95 were found in rafts and shifted from rafts after αSyn incubation of slices (Supplementary Fig. 2a and b), indicating an effect of extracellular αSyn that is independent from the presence of the endogenous protein.

We next investigated if the change in raft-partitioning of NR2b subunit and PSD-95 in response to αSyn could affect their interaction. Brain slices incubated with or without αSyn were lysed, immunoprecipitated with anti-NR2b antibody and analyzed for co-immunoprecipitated PSD-95. As expected, the amount of PSD-95 co-immunoprecipitated with NR2b in the presence of extracellular αSyn was decreased by ~40% with respect to control (Fig. 2d and e).

Because the interaction between NR2b and PSD-95 is regulated by phosphorylation of S1480 in the PDZ binding domain of NR2b, the increase in phosphorylation of S1480 resulting in the disruption of their binding (Chen and Roche, 2007); we analyzed the phosphorylation state of NR2b in cortico-striatal brain slices incubated with or without αSyn for 2 h. A ~35% increase in NR2b phosphorylation of S1480 was observed in αSyn-treated sample, while the total level of NR2b was unaltered (Fig. 2f and g). To understand if this effect was dependent on αSyn-driven dispersion of lipid rafts, we used methyl-beta cyclodextrin (MβCD) to decrease cholesterol content. Indeed, we found that cholesterol reduction induced by MβCD correlated with increased phosphorylation of NR2b (Fig. 2h and i).

3.3. Inhibition of CK2 prevents αSyn effect on post-synaptic proteins

CK2, that phosphorylates S1480 of NR2b, may therefore be a potential target to restore the interaction between PSD-95 and the NMDAR subunit, lost upon αSyn treatment, and the ensuing defects in post-synaptic activity. On the other hand, αSyn-driven de-localization of PSD-95 and NR2b might also be prevented by cholesterol loading that would restore raft platforms on the membrane, as it was shown for the activation of $Ca_v2.2$ (Ronzitti et al., 2014). To assess this possibility we used 4,5,6,7-tetrabromobenzotriazole (TBB), a specific CK2 inhibitor (Sarno et al., 2001), and cholesterol-loaded methyl-beta cyclodextrin (chol-MβCD) to increase cholesterol content. Brain slices were incubated with αSyn, either alone or with the addition of 1 μM TBB or 1.3 mg/ml chol-MβCD. We found that in slices incubated with αSyn + TBB, NR2b phosphorylation was decreased to control levels. Conversely, cholesterol had no effect on αSyn-induced phosphorylation of NR2b (Fig. 3a and b). Similarly, in slices incubated with αSyn + TBB, NR2b co-immunoprecipitated the same amount of PSD-95 as in control, while in the presence of cholesterol, αSyn-dependent decrease of PSD-95 binding to NR2b was unaffected (Fig. 3c and d). TBB and cholesterol were also analyzed for their ability to prevent αSyn effect on the dispersion of proteins from rafts. In the presence of TBB, the percentage of PSD-95 and NR2b recovered in raft fractions was similar to control, while, consistently with the previous results, the incubation with cholesterol did not prevent αSyn-induced re-localization of the two proteins in cholesterol-poor domains (Fig. 3e and f). Taken together, these results indicate that the decrease in cholesterol-rich domains induced by αSyn is responsible of the activation of CK2 and disruption of NR2b/PSD-95 complex, that cannot however be restored by massive cholesterol loading of the membrane.

3.4. Extracellular αSyn affects postsynaptic structure and function

Since the function of synapses crucially depends on the proper alignment of presynaptic and postsynaptic specializations, and on the targeting of synaptic machinery at appropriate sites (Baron et al., 2006), it is conceivable that perturbation of the correct localization of post-synaptic proteins could lead to defects in synapse formation and maintenance. Given αSyn effect on the raft localization of postsynaptic components we asked if αSyn could trigger changes in the juxtaposition of pre- and post-synaptic proteins by analyzing the co-localization of PSD-95 with the pre-synaptic markers synaptophysin and synaptotagmin-1 (Fig. 4a). In striatal slices incubated for 2 h with αSyn we found a ~40% decrease in co-localization between synaptophysin and PSD-95 and between synaptotagmin-1 and PSD-95 (Fig. 4b). Also in this case, the incubation of slices with TBB was able to restore the co-localization of pre- and post-synaptic proteins to control levels, while cholesterol loading of slices was not effective (Fig. 4a and b). These results were consistent with a possible alteration of synaptic functionality as a consequence to αSyn exposure. To investigate this possibility, synaptic plasticity was evaluated using a protocol of chemically-induced form of LTP (Lu et al., 2001; Menna et al., 2013), which was shown to result in a significant increase in the density and size of PSD-95 positive puncta (Fossati et al., 2015; Menna et al., 2013). Neuronal cultures were incubated with high doses of glycine for 3 min, followed by washout and immunolabeling for PSD-95, v-Glut1 and tubulin after a 1 h recovery period. Notably, in neurons exposed to extracellular αSyn this protocol did not induce increases in either the size or the density of PSD-95 positive puncta (Fig. 4c–e). The lack of potentiation upon exposure to extracellular αSyn was also confirmed by electrophysiological recordings of mEPSCs. Indeed, while both the frequency and amplitude of mEPSCs significantly increased 35 min after glycine application in vehicle-treated neurons, no potentiation occurred in αSyn-treated neurons (Fig. 4f–h). Interestingly, application of forskolin, an activator of adenylyl cyclase, was still able to induce a structural potentiation in αSyn-treated neurons as shown by the increase of the density and the size of PSD-95 puncta (Fig. 4i–k), indicating that the signaling pathway downstream NMDAR activation is not impaired upon exposure to extracellular αSyn. Indeed electrophysiological recordings of AMPA-mediated miniature events were not affected by αSyn treatment (black vs red bars in Fig. 4g and h); also the partitioning of GluA1 (Fig. 2a and c) exhibited no changes after αSyn treatment, indicating that αSyn specifically affects NMDA receptors.

3.5. Extracellular αSyn acutely increases the density of PSD-95 puncta raising cytosolic calcium

To investigate whether extracellular αSyn impacts formation and/or maintenance of the postsynaptic compartment we evaluated the density of PSD-95 puncta upon overexpression of PSD-95, a procedure which results in the marked increase in synapse number (Nikonenko et al., 2008). Cortical neurons at 17 DIV were co-transfected with PSD-95-RFP to identify PSD-95 puncta and with GFP to visualize the neurites. After 3 days from transfection, neurons were incubated with or without αSyn, or αSyn + TBB or αSyn + chol-MβCD for 2 h and fixed.

Please cite this article as: Emanuele, M., et al., Exogenous Alpha-Synuclein Alters Pre- and Post-Synaptic Activity by Fragmenting Lipid Rafts, EBioMedicine (2016), http://dx.doi.org/10.1016/j.ebiom.2016.03.038

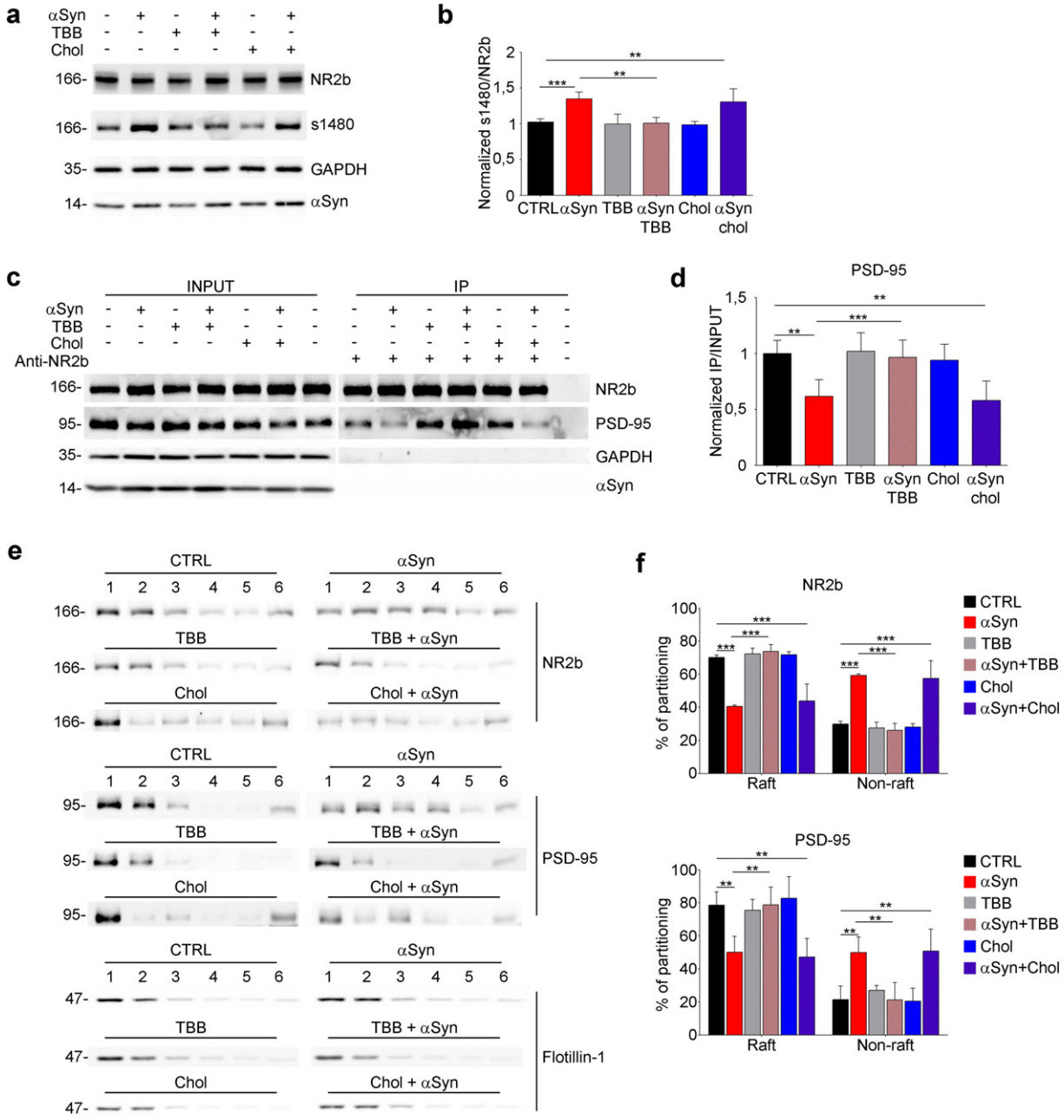

Fig. 3. TBB prevents αSyn effect on the localization of PSD-95 and NR2b and on their interaction. (a) Immunoblot showing S1480 phosphorylation level in sample from brain slices incubated with 5 μM αSyn, 1 μM TBB, 5 μM αSyn + 1 μM TBB, 1.3 mg/ml chol-MβCD or 5 μM αSyn + 1.3 mg/ml chol-MβCD. Overlay was performed with the antibodies indicated on the right. (b) Quantification by densitometry of S1480 phosphorylation level normalized on NR2b. n = 5. (c) Immunoblot showing co-immunoprecipitation with anti-NR2B antibody from cortico-striatal brain slices incubated as in a. The seven left lanes show extracts (INPUT; 10% of the total). The seven right lanes show immunoprecipitates (IP). (d) Quantitative evaluation by densitometry of immunoprecipitated PSD-95 band normalized on the INPUT. n = 5. (e) Immunoblot of sucrose gradients loaded with extracts derived from cortico-striatal brain slices incubated as in a, showing the distribution of proteins in raft (fractions 1 and 2) and non-raft (fractions 3–6). (f) Quantitative evaluation by densitometry of protein content in raft or non-raft fractions expressed as percentage of the total protein amount calculated as in Fig. 2c. Data are expressed as mean ± SEM. Statistical significance determined by 2way-ANOVA. n = 4. Data are expressed as mean ± SEM (b, d, f). Statistical significance determined by 1way-ANOVA (b, d), or 2way-ANOVA (f). $^{**}p < 0.01$, $^{***}p < 0.001$.

Consistently with the decrease of PSD-95/NR2b clustering in rafts, a ~27% decrease of PSD-95 density was observed after 2 h of αSyn treatment (Fig. 5a and b), indicating that the process of synapse formation induced by PSD-95 overexpression is impaired by extracellular αSyn. Conversely, a ~20% increase in PSD-95 staining was evident after 30 min of exposure to αSyn suggesting the occurrence of a biphasic effect of αSyn on synaptic components (Fig. 5c and d). Surprisingly, however, while TBB prevented αSyn-induced decrease in the number of PSD-95 puncta at 2 h, it was ineffective on αSyn-induced increase of PSD-95 puncta at 30 min, while, on the contrary, cholesterol loading was able to prevent only the short term effect of αSyn (Fig. 5a–d). Calcium chelation by EGTA also prevented the short term effect of αSyn, being ineffective on the later decrease of PSD puncta (Fig. 5a–d).

αSyn is also a target for CK2 that phosphorylates it in serine 129, resulting in increased toxicity of the protein (Hara et al., 2013). In order to understand if the defects in synaptic connectivity and the disorganization of the post-synaptic density were caused by αSyn hyperphosphorylation, we employed αSynS129E-GFP, a fluorescently tagged phosphomimetic αSyn construct. Neurons expressing phosphorylated αSyn exhibited the same amount of PSD-95 puncta compared to control neurons, and the addition of extracellular αSyn was affecting PSD-95 density in both cases (Supplemental Fig. 2a and b).

Please cite this article as: Emanuele, M., et al., Exogenous Alpha-Synuclein Alters Pre- and Post-Synaptic Activity by Fragmenting Lipid Rafts, EBioMedicine (2016), http://dx.doi.org/10.1016/j.ebiom.2016.03.038

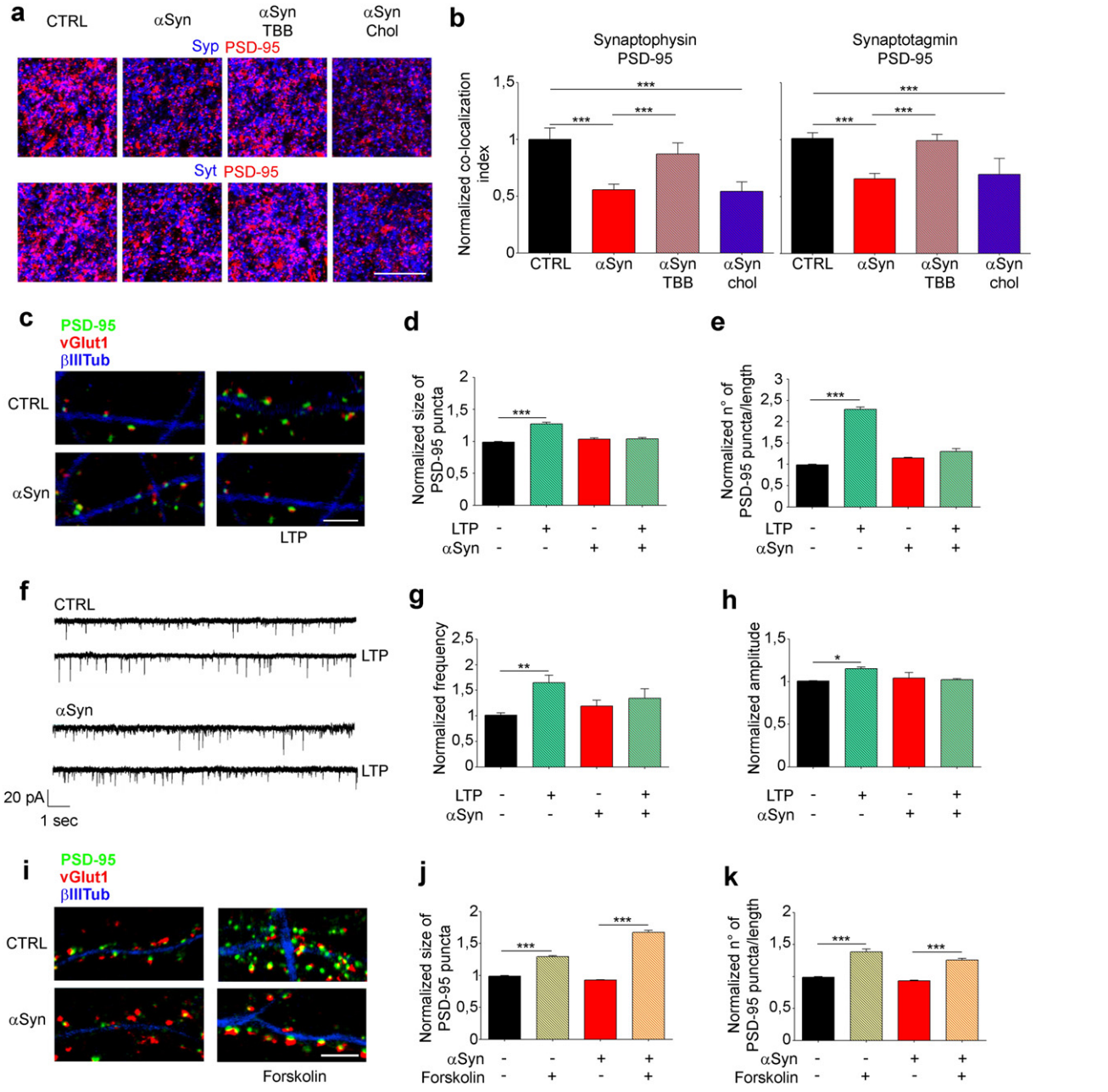

Fig. 4. Extracellular αSyn hampers long term potentiation in a NMDAR-dependent way. (a) Confocal images of cortico-striatal brain slices incubated without or with 5 μM αSyn, 1 μM TBB, 5 μM αSyn + 1 μM TBB, 1.3 mg/ml chol-MβCD or 5 μM αSyn + 1.3 mg/ml chol-MβCD and immunostained for synaptophysin, synaptotagmin-1 and PSD-95. Scale bar = 150 μm. (b) Statistical analysis of the normalized co-localization index of pre- and post-synaptic proteins in brain slices incubated without or with 5 μM αSyn, 1 μM TBB, 5 μM αSyn + 1 μM TBB, 1.3 mg/ml chol-MβCD or 5 μM αSyn + 1.3 mg/ml chol-MβCD. The co-localization index is PSD-95-synaptophysin: n = 50 from 5 independent experiments. PSD-95-synaptotagmin-1: n = 46 from 5 independent experiments. (c) Representative images of rat hippocampal neurons incubated without or with 5 μM αSyn before and after performing a chemical LTP procedure. Cultures were stained for PSD-95 (green), v-Glut1 (red) and tubulin (blue). Scale bar: 6 μm. (d) Quantification of the mean size of PSD-95 positive clusters. (e) Quantification of the density of PSD-95 puncta. n (fields/condition) = 50 from 3 independent experiments. (f) Representative mEPSC traces of electrophysiological recordings of mEPSCs before and after chemical LTP induction in vehicle or αSyn-treated neurons. (g) Quantification of normalized mEPSC frequency. (h) Quantification of normalized mEPSC amplitude n = 20, 22, 13, 22 from 3 independent experiments. (i) Representative images of rat hippocampal neurons incubated without or with 5 μM αSyn before and after performing forskolin- induced LTP. Cultures were stained as in c. Scale bar: 6 μm. (j) Quantification of the mean size of PSD-95 positive clusters. (k) Quantification of the density of PSD-95 puncta. n (fields/condition) = 50 from 3 independent experiments. Data are expressed as mean ± SEM (b, d, e, g, h, j, k). Statistical significance determined by 1way-ANOVA (b, d, e, j, k), or by t-test (g, h), *p < 0,05, **p < 0.01,***p < 0.001. (For interpretation of the references to color in this figure legend, the reader is referred to the web version of this article.)

Based on our previous results indicating an early activation of $Ca_v2.2$ calcium channels with ensuing increased dopamine release upon αSyn treatment (Ronzitti et al., 2014), we reasoned that the increase in the density of PSD-95 puncta observed after 30 min of incubation with αSyn and that is inhibited by EGTA, could be determined, in an activity-dependent manner (De Roo et al., 2008), by an increase of neurotransmitter release consequent to the enhanced calcium influx. To assess this possibility, we evaluated basal calcium entry after incubation of neurons with αSyn by analyzing the recruitment to the PM of Extended-Synaptotagmin1 (E-Syt1), a protein that participates in the tethering of ER with PM in a manner dependent on cytosolic Ca^{2+} elevation (Giordano et al., 2013; Min et al., 2007). Cortical neurons at 14 DIV expressing E-Syt1-GPF were imaged in time lapse using total internal reflection fluorescence microscopy (TIRF) that allows acquisition of signals at a distance of 100 nm from the PM. The high sensitivity of the system would detect changes in calcium influx that might arise after αSyn incubation of

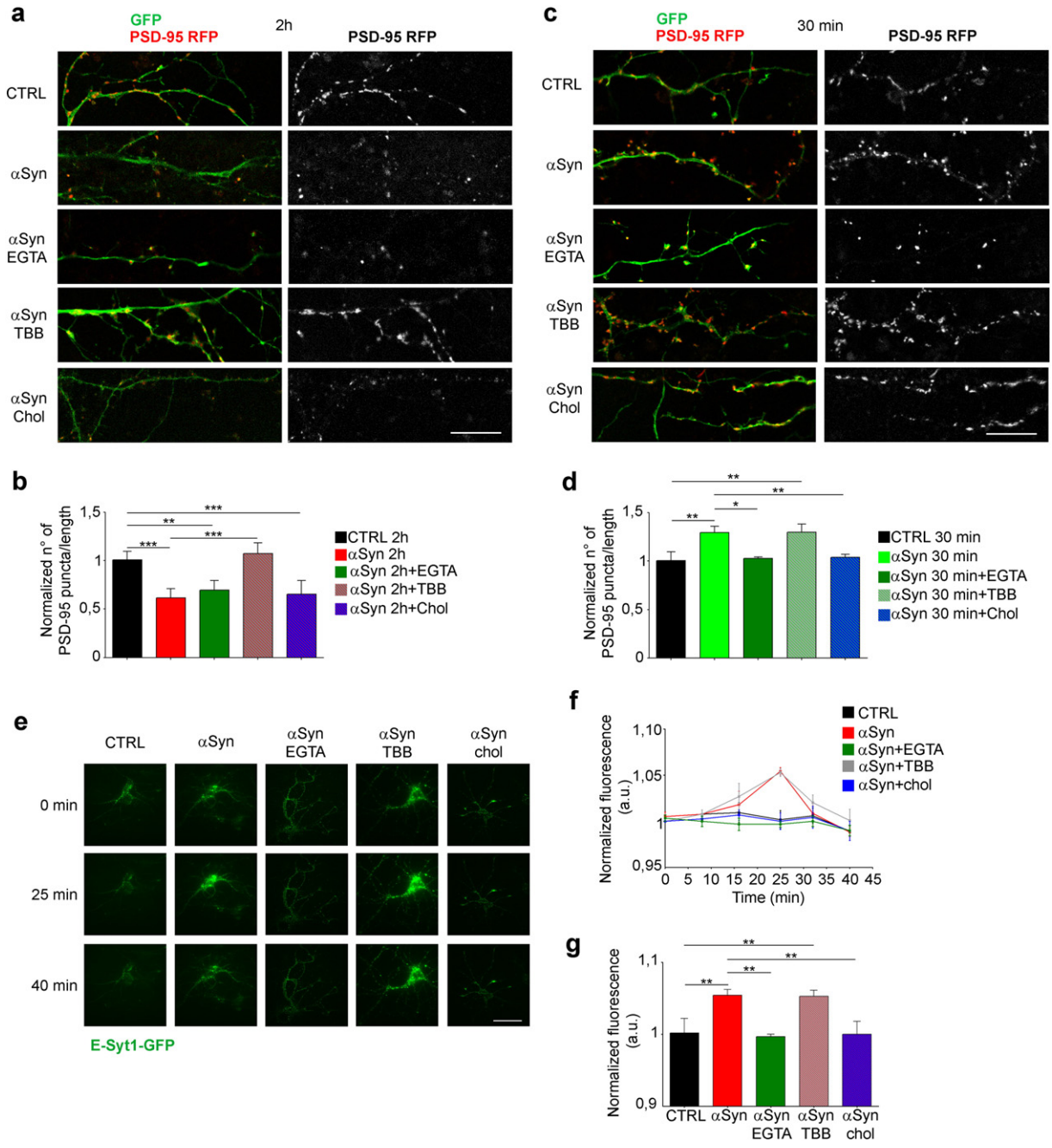

Fig. 5. Cholesterol-loaded MβCD and TBB prevent αSyn biphasic effect on synapse formation and maintenance. (a) Representative images of dendrites of cortical neurons double-transfected with GFP and PSD-95-RFP, and incubated for 2 h without or with 5 μM αSyn, 5 μM αSyn + 100 EGTA μM, 1 μM TBB, 5 μM αSyn + 1 μM TBB, 1.3 mg/ml chol-MβCD or 5 μM αSyn + 1.3 mg/ml chol-MβCD, and fixed. Scale bar: 20 μm. (b) Quantitative evaluation of PSD-95 signal indicated as number of puncta/length, normalized on the control. n = 33. (c) Representative images of dendrites of cortical neurons double-transfected with GFP and PSD-95-RFP, and incubated for 30 min as in a, and fixed. Scale bar: 20 μm. (d) Quantitative evaluation of PSD-95 signal indicated as number of puncta/length, normalized on the control. n = 33. (e) Representative TIRF images of cortical neurons expressing E-Syt1-GPF incubated without (CTRL) or with 5 μM αSyn, 5 μM αSyn + 100 μM EGTA, 5 μM αSyn + 1 μM TBB or 5 μM αSyn + 1.3 mg/ml chol-MβCD and imaged in time lapse at a distance of 100 nm from the plasma membrane. Scale bar: 200 μm. (f) Averaged fluorescence intensity profiles, values at each time point are normalized on the first value after subtraction of the background fluorescence value. (g) Quantification of the peak fluorescence value, reached after 25 min, and normalized on control. n = 6 from 3 independent experiments. Data are expressed as mean ± SEM (b, d, f, g). Statistical significance determined by 1way-ANOVA (b, d, f, g). **p < 0.01, ***p < 0.001.

neurons. Neurons treated with αSyn or αSyn + TBB showed an increase of E-Syt1 fluorescence starting 10 min after incubation, with a peak of fluorescence reached after 25 min. The movement of E-Syt1 toward the PM was indicative of an increase in cytosolic calcium, as shown by the inhibition of the process in the presence of EGTA (Fig. 5e–g). On the other hand, control neurons and neurons incubated with αSyn + chol-MβCD did not show any increase in fluorescence (Fig. 5e–g), indicating that αSyn-driven increase in intracellular Ca^{2+} could be prevented by cholesterol loading.

3.6. Extracellular αSyn increases basal and evoked SVs' mobilization and cholesterol prevents its effect

The observed increase in calcium influx due to extracellular αSyn prompted us to evaluate mobilization and fusion of SVs using neurons transfected with VAMP2-GFP and analyzed by TIRF microscopy. Incubation of neurons with αSyn and αSyn + TBB resulted in the increase in fluorescence intensity after 10 min, followed after 30 min by a fluorescence decrease, which reached control values in 50 min

Please cite this article as: Emanuele, M., et al., Exogenous Alpha-Synuclein Alters Pre- and Post-Synaptic Activity by Fragmenting Lipid Rafts, EBioMedicine (2016), http://dx.doi.org/10.1016/j.ebiom.2016.03.038

(Fig. 6a–c). Neurons incubated with αSyn + chol-MβCD did not display any difference compared to controls, indicating that the pre-synaptic effects of αSyn could be prevented by cholesterol loading. Further, we measured the possible alteration in evoked mobilization and fusion of SVs. 14 DIV cortical neurons expressing VAMP2-GPF were incubated for 10, 20, 30 or 60 min with or without αSyn, alone or together with TBB or chol-MβCD (Fig. 6d), and stimulated with 100 action potentials (APs) at 20 Hz. Using TIRF we followed the entire cycle of vesicles' exocytosis (Zenisek et al., 2000). The fluorescence signal increased with the stimulus (0 ms) and started to decrease after 100 ms, disappearing completely after 400 ms (Fig. 6d and e, 0 min). Upon incubation with αSyn or αSyn + TBB for 20 to 30 min, the fluorescence signal at 100 ms increased in respect to control (Fig. 6e, 20 min, 30 min) and was calculated to be ~50% higher (Fig. 6f). After 60 min of incubation with αSyn the signal was undetectable at all time points (Fig. 6d, 60 min). In all conditions where an increase of vesicle mobilization due to αSyn was visible, the treatment of neurons with chol-MβCD was able to prevent αSyn effect, while TBB was not (Fig. 6d–f). The increase in VAMP2 signal was suggestive of increased vesicles' mobilization, and the possibility of an impairment of vesicle fusion was excluded by the complete absence of the signal after 60 min of incubation with αSyn, indicative of an exhaustion of SVs. Also at this time point the treatment of neurons with chol-MβCD was able to prevent αSyn effect, while TBB was not (Fig. 6d and e, 60 min). Consistently, ultrastructural analysis showed that the total number of SVs per synapse was reduced of ~36% in slices incubated with αSyn in respect with control, and cholesterol loading prevented this effect (Fig. 7a and b). In slices incubated with αSyn, the space of synaptic cleft was not affected (Fig. 7c), whereas the PSD area was decreased of ~33% compared to control (Fig. 7d), consistently with the altered clustering of PSD95/NR2b complex induced by αSyn. Incubation with TBB prevented this effect (Fig. 7d).

Based on our finding of reduction of synaptic contacts and PSD area, we wondered if αSyn could affect dendritic spines' morphology. Fluorescent lipid labeling of slices (Fig. 7e) highlighted a significant, albeit

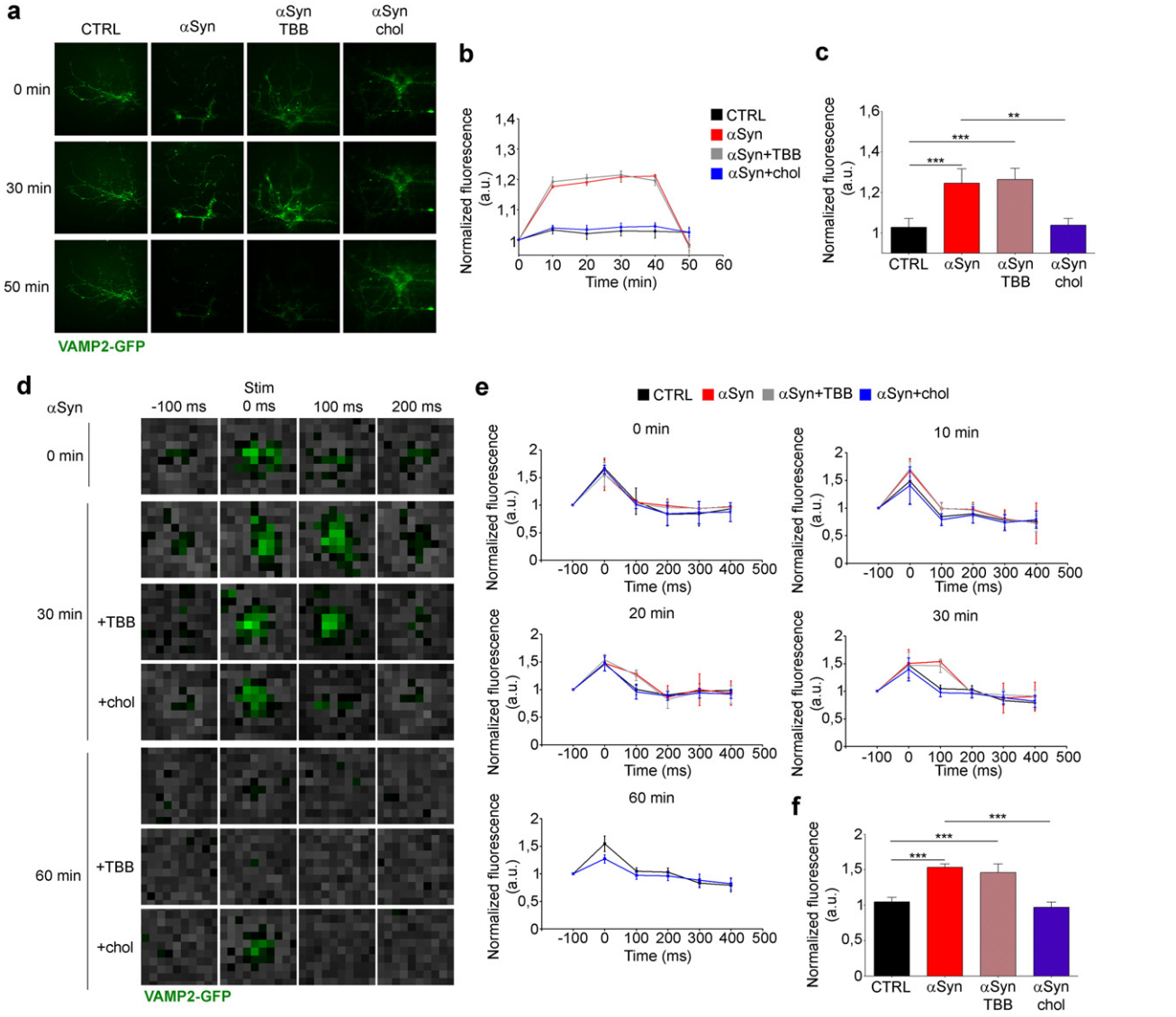

Fig. 6. Extracellular αSyn increases basal and evoked SV dynamics and alters the synaptic architecture. (a) TIRF images of cortical neurons expressing VAMP2-GPF incubated with 5 μM αSyn, 5 μM αSyn + 1 μM TBB or 5 μM αSyn + 1.3 mg/ml chol-MβCD and imaged in time lapse at a distance of 100 nm from the plasma membrane. Scale bar: 200 μm. (b) Averaged fluorescence intensity profiles normalized as in Fig. 5f. (c) Quantification of fluorescence intensity at 30 min, normalized on control. n = 8 from 3 independent experiments. (d) TIRF images of cortical neurons expressing VAMP2-GPF incubated as in a for 30 or 60 min. The green color represents VAMP2-GFP approaching to the PM. Images were taken before stimulation (−100 ms), during stimulation (0 ms) and after stimulation (100 ms, 200 ms). Scale bar: 400 nm. (e) Averaged fluorescence intensity profiles of samples incubated as in a, for 10, 20, 30 or 60 min, the values at each time point are normalized on the first value. (f) Quantification of the peak fluorescence value, reached after 100 ms in samples incubated as in a, for 30 min, normalized on control value. n = 9 from 4 independent experiments. Data are expressed as mean ± SEM (b, c, e, f). Statistical significance determined by 1way-ANOVA (c, f). $^{**}p < 0.01$, $^{***}p < 0.001$. (For interpretation of the references to color in this figure legend, the reader is referred to the web version of this article.)

Please cite this article as: Emanuele, M., et al., Exogenous Alpha-Synuclein Alters Pre- and Post-Synaptic Activity by Fragmenting Lipid Rafts, EBioMedicine (2016), http://dx.doi.org/10.1016/j.ebiom.2016.03.038

slight, ~18% decrease in both the number and size of spines after 2 h of treatment with αSyn (Fig. 7f and g), possibly as a result of the collapse of the PSD area.

Taken together these results indicate that extracellular αSyn affects pre- and post-synaptic morphology and activity through fragmentation of lipid rafts and consequent de-localization of membrane associated proteins.

4. Discussion

Our study provides evidence of the pathological role that high concentration of monomeric αSyn in the extracellular milieu has on synaptic activity. It has been calculated that the concentration of αSyn in the presynaptic bouton is ~20 μM (Wilhelm et al., 2014). This amount is doubled or tripled in the genetic forms of PD, and, due to polymorphisms in the *SNCA* gene found in PD patients, high levels of αSyn are also involved in the pathogenesis of the sporadic form of PD (Chiba-Falek et al., 2006; Farrer et al., 2004). Such a high concentration of αSyn would lead to high level of the protein released in the interstitial brain tissue that will accumulate in time, and we can hypothesize that high amount of αSyn will be present in the synaptic cleft. It was shown a dose-dependency of the effect of human wt αSyn on the activation of $Ca_v2.2$ channels (Ronzitti et al., 2014). Our results indicate that αSyn influences synaptic function by fragmentation of lipid rafts in a dose dependent-way and by de-localization of lipid raft-associated proteins. Lipid rafts arrange into large, stable membrane platforms rich in cholesterol, that recruit downstream signaling molecules (Dinic et al., 2015). In the postsynaptic compartment, PSD proteins, such as PSD-95, are associated with lipid rafts (Perez and Bredt, 1998), while in the presynaptic terminal, components of exocytotic machinery and calcium channels are raft-associated (Chamberlain et al., 2001; Robinson et al., 2010), suggesting a role for rafts in the regulation of neurotransmission. Therefore it is conceivable that αSyn-driven changes in the correct localization and trafficking of proteins along the PM could deeply alter synaptic function. The selectivity of αSyn effect on the movement of membrane-associated proteins out of lipid rafts, is possibly dependent on the different strength of association of

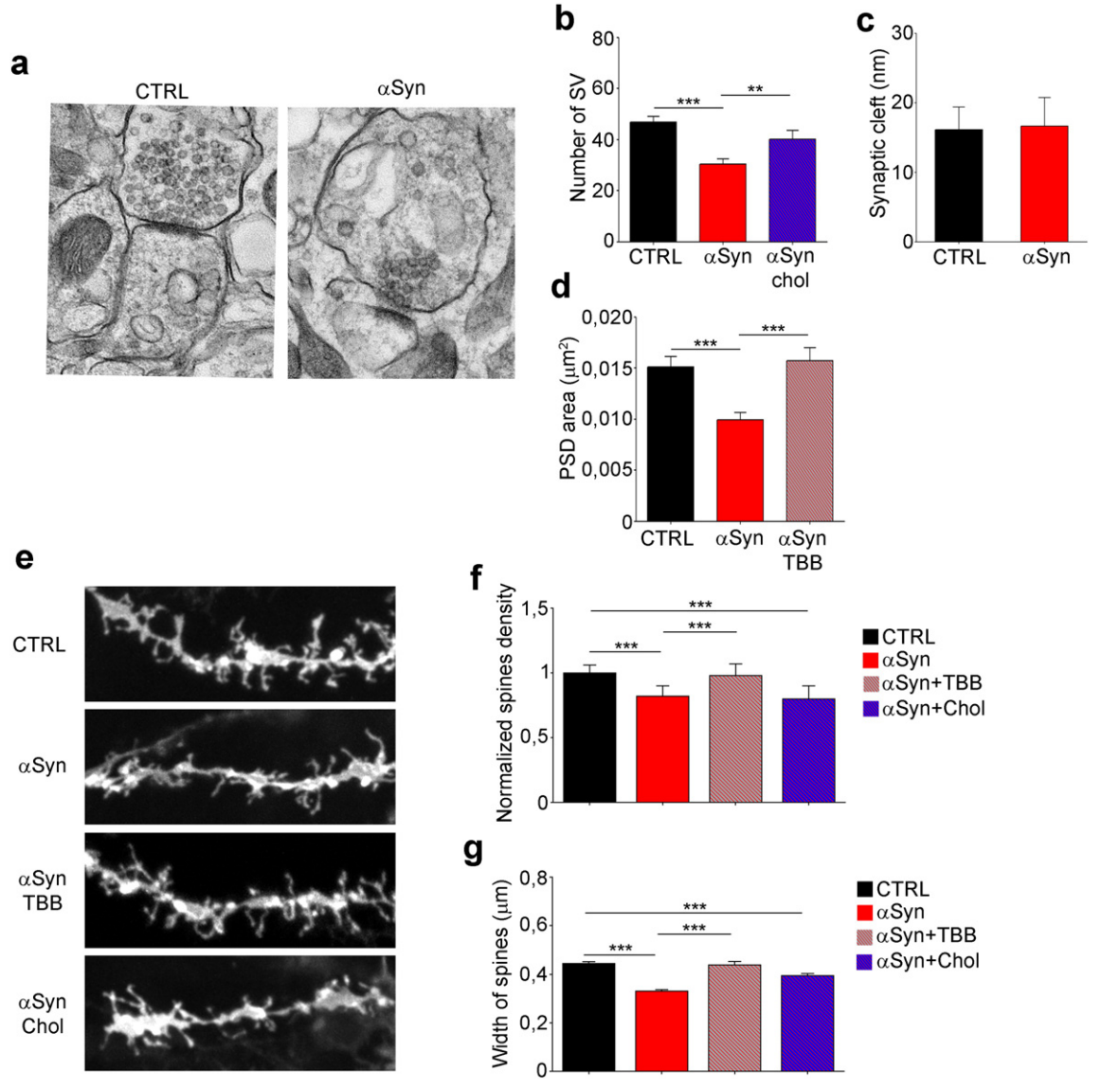

Fig. 7. Extracellular αSyn alters the synaptic architecture and reduces the number and size of dendritic spines. (a) Representative electron micrographs of synapses in cortico-striatal brain slices incubated (right panel) or not (left panel) with 5 μM αSyn for 2 h. (b) Quantitative evaluation of the number of SVs. n = 92, 105, 59. (c) Quantitative evaluation of the synaptic cleft width. n = 76, 63. (d) Quantitative evaluation of the PSD area. n = 96, 114, 50. (e) Representative confocal images of dendritic segments of cortico-striatal brain slices, incubated without or with 5 μM αSyn, 1 μM TBB, 5 μM αSyn + 1 μM TBB, 1.3 mg/ml chol-MβCD or 5 μM αSyn + 1.3 mg/ml chol-MβCD and labeled with DiI. (f) Quantification of spine density indicated as number of spines/unit length (μm) of parent dendrite, normalized on the control. n = 150 fields from 3 independent experiments. (g) Quantification of the width of the spines. n = 150 fields from 3 independent experiments. Data are expressed as mean ± SEM (b, c, d, f, g). Statistical significance determined by 1way-ANOVA (b, d, f, g) or t-test (c). $^{**}p < 0.01$, $^{***}p < 0.001$.

Please cite this article as: Emanuele, M., et al., Exogenous Alpha-Synuclein Alters Pre- and Post-Synaptic Activity by Fragmenting Lipid Rafts, EBioMedicine (2016), http://dx.doi.org/10.1016/j.ebiom.2016.03.038

proteins with the membrane, or on the differential role of lipid rafts, presynaptic proteins or cytoskeletal elements in the maintenance of protein clusters, and in the confinement of distinct proteins in their specific site of localization.

We focused our analysis on PSD-95, which, interacting with a variety of receptors and ion channels, determines the size and strength of synapses (Scannevin and Huganir, 2000). The described de-localization of PSD-95 and NR2b subunit of NMDAR from lipid rafts could explain some aspects of αSyn-related pathology. Abnormalities in the subcellular localization of PSD-associated proteins were shown in 6-OHDA-lesioned rat model of PD (Nash et al., 2005). Moreover defects in the localization of PSD-95, which promotes recycling of D1 dopamine receptor (Sun et al., 2009), could lead to altered receptor activity. On the other hand, dysfunction of NMDAR contributes to neurodegenerative disorders. It was demonstrated that inhibition of LTP triggered by β-amyloid depends on altered activation of NR2b (Li et al., 2011). In a transgenic mouse model of PD it was found that decreased hippocampal LTP, which correlates with cognitive deficits, is associated with impaired neurotransmission and decreased NR2a/NR2b ratio (Costa et al., 2012). The dispersion of PSD proteins' clusters was also highlighted by our data showing decreased co-localization between pre- and post-synaptic proteins, by electron microscopy analysis of PSD area, which resulted smaller upon exposure of brain slices to αSyn, and by the observed decrease in the size and number of dendritic spines, indicating a pathogenic role for αSyn in the maintenance of synaptic architecture and synaptic contacts.

SV trafficking is affected in αSyn knocked out and transgenic mice, suggesting αSyn role in neurotransmission (Esposito et al., 2012). At short time of incubation of neurons with αSyn, the observed increase in SV mobilization and fusion may correlate to the increased calcium influx. Instead, at later time points of exposure to αSyn, an exhaustion of SVs was observed, as showed by ultrastructural analysis and TIRF microscopy.

We demonstrated the ability of cholesterol loading and CK2 inhibition to prevent the short and long-term effects of αSyn, respectively. In our previous study, the increased activation of $Ca_v2.2$, and ensuing calcium influx induced by αSyn, was prevented by cholesterol loading, which would restore raft platforms on the membrane. Consistently, the increase in basal and evoked SV fusion and the movement of E-Syt1 near the PM, which are directly related to calcium influx, were prevented by cholesterol. Similarly, cholesterol was able to prevent the activity-dependent increase of PSD-95 puncta after 30 min of incubation with αSyn. Recently, alterations were described in the lipid composition of the frontal cortex from PD patients, in particular the concentration of phosphatidylserine and phosphatidylinositol was found increased in PD brains. (Fabelo et al., 2011). E-Syts form complexes that mediate ER/PM contacts and are implicated in PM replenishment with phosphatidylinositol (Chang et al., 2013). Such contacts are regulated via the Ca^{2+}-sensing property of E-Syt1. We showed increased tethering of E-Syt1 with PM during the incubation of neurons with αSyn, result that, besides being an indication of increased calcium entry, might also represent the mechanism underlying αSyn effect on PM composition.

On the other hand, CK2 inhibition prevents αSyn-induced long term effect on the post-synaptic compartment. CK2 is a constitutively active serine/threonine kinase that can be regulated by interaction with proteins, and by autophosphorylation (Litchfield, 2003). CK2 is known to interact with cytoskeletal protein that might target it to specific sites, and regulate its activity depending on its subcellular localization (Faust et al., 1999). The mechanism that leads to CK2-dependent phosphorylation of S1480 of NR2b upon exposure to αSyn is possibly due to the decrease in raft size and, similarly, cholesterol depletion by MβCD also leads to activation of CK2. It was reported the presence of CK2 in lipid raft preparations from rat brain (Gil et al., 2011), and we can hypothesize that αSyn, perturbing the organization of the membrane, might provoke an increased, or unregulated, interaction of CK2 with its substrate, i.e. NR2b, which in turn become phosphorylated, detaching from PSD-95. The protective effect of CK2 inhibition would be due to its action downstream of αSyn activity.

Therefore replenishment of membranes with cholesterol could prevent αSyn effect on calcium influx and SV mobilization, mechanically counteracting the activation of $Ca_v2.2$ calcium channels. On the other hand, cholesterol loading of the PM was not enough to restore PSD-95 binding to NMDAR subunit which requires a dynamically controlled interaction with CK2. The maintenance of the correct localization of the two post-synaptic proteins and of the structure of synaptic contacts, which were disrupted by αSyn, was instead achieved by inhibition of CK2.

Author contributions

M.E. and A.E. performed and analyzed biochemical and imaging experiments. S.C. and M.C. performed and analyzed proteomic experiments. F.A. performed and analyzed electrophysiological recordings. F.S. and E.M. performed and analyzed immunostaining experiments for the evaluation of LTP. T.C. and R.M. performed and analyzed electron microscopy experiments. S.S. and C.C. performed and analyzed AFM experiments. M.E. and E.C. conceived the project. M.E., E.M. and E.C. contributed to its conceptualization. E.C. directed it throughout and secured funding. M.E. M.M. and E.C. wrote the manuscript.

Conflict of interest

The authors declare that they have no conflict of interest.

Acknowledgments

We thank Brett Lauring (Columbia University, NY) for αSyn plasmids, Pietro De Camilli for E-Syt1-GFP plasmid and Flavia Valtorta for VAMP2-GFP plasmid.

This work was partially supported by Telethon Foundation GGP10109 (to E.C.), PRIN 2010-2011 2010JFYFY2_008 (to M.M.) and CNR Progetto Bandiera InterOmics (to E.M.).

Appendix A. Supplementary data

Supplementary data to this article can be found online at http://dx.doi.org/10.1016/j.ebiom.2016.03.038.

References

Baron, M.K., Boeckers, T.M., Vaida, B., Faham, S., Gingery, M., Sawaya, M.R., Salyer, D., Gundelfinger, E.D., Bowie, J.U., 2006. An architectural framework that may lie at the core of the postsynaptic density. Science 311, 531–535.

Bickel, P.E., Scherer, P.E., Schnitzer, J.E., Oh, P., Lisanti, M.P., Lodish, H.F., 1997. Flotillin and epidermal surface antigen define a new family of caveolae-associated integral membrane proteins. J. Biol. Chem. 272, 13793–13802.

Borghi, R., Marchese, R., Negro, A., Marinelli, L., Forloni, G., Zaccheo, D., Abbruzzese, G., Tabaton, M., 2000. Full length alpha-synuclein is present in cerebrospinal fluid from Parkinson's disease and normal subjects. Neurosci. Lett. 287, 65–67.

Butchbach, M.E.R., Tian, G., Guo, H., Lin, C.L.G., 2004. Association of excitatory amino acid transporters, especially EAAT2, with cholesterol-rich lipid raft microdomains: importance for excitatory amino acid transporter localization and function. J. Biol. Chem. 279, 34388–34396.

Chamberlain, L.H., Burgoyne, R.D., Gould, G.W., 2001. SNARE proteins are highly enriched in lipid rafts in PC12 cells: implications for the spatial control of exocytosis. Proc. Natl. Acad. Sci. U. S. A. 98, 5619–5624.

Chang, C.L., Hsieh, T.S., Yang, T.T., Rothberg, K.G., Azizoglu, D.B., Volk, E., Liao, J.C., Liou, J., 2013. Feedback regulation of receptor-induced Ca2 + signaling mediated by E-Syt1 and Nir2 at endoplasmic reticulum-plasma membrane junctions. Cell Rep. 5, 813–825.

Chen, B.S., Roche, K.W., 2007. Regulation of NMDA receptors by phosphorylation. Neuropharmacology 53, 362–368.

Chiba-Falek, O., Lopez, G.J., Nussbaum, R.L., 2006. Levels of alpha-synuclein mRNA in sporadic Parkinson disease patients. Mov. Disord. 21, 1703–1708.

Chung, H.J., Huang, Y.H., Lau, L.F., Huganir, R.L., 2004. Regulation of the NMDA receptor complex and trafficking by activity-dependent phosphorylation of the NR2B subunit PDZ ligand. J. Neurosci. 24, 10248–10259.

Costa, C., Sgobio, C., Siliquini, S., Tozzi, A., Tantucci, M., Ghiglieri, V., Di Filippo, M., Pendolino, V., de Iure, A., Marti, M., et al., 2012. Mechanisms underlying the

impairment of hippocampal long-term potentiation and memory in experimental Parkinson's disease. Brain 135, 1884–1899.
De Roo, M., Klauser, P., Mendez, P., Poglia, L., Muller, D., 2008. Activity-dependent PSD formation and stabilization of newly formed spines in hippocampal slice cultures. Cereb. Cortex 18, 151–161.
Desplats, P., Lee, H.J., Bae, E.J., Patrick, C., Rockenstein, E., Crews, L., Spencer, B., Masliah, E., Lee, S.J., 2009. Inclusion formation and neuronal cell death through neuron-to-neuron transmission of alpha-synuclein. Proc. Natl. Acad. Sci. U. S. A. 106, 13010–13015.
Dettmer, U., Selkoe, D., Bartels, T., 2016. New insights into cellular alpha-synuclein homeostasis in health and disease. Curr. Opin. Neurobiol. 36, 15–22.
Dinic, J., Riehl, A., Adler, J., Parmryd, I., 2015. The T cell receptor resides in ordered plasma membrane nanodomains that aggregate upon patching of the receptor. Sci. Rep. 5, 10082.
Diogenes, M.J., Dias, R.B., Rombo, D.M., Vicente Miranda, H., Maiolino, F., Guerreiro, P., Nasstrom, T., Franquelim, H.G., Oliveira, L.M., Castanho, M.A., et al., 2012. Extracellular alpha-synuclein oligomers modulate synaptic transmission and impair LTP via NMDA-receptor activation. J. Neurosci. 32, 11750–11762.
Esposito, G., Ana Clara, F., Verstreken, P., 2012. Synaptic vesicle trafficking and Parkinson's disease. Dev. Neurobiol. 72, 134–144.
Fabelo, N., Martin, V., Santpere, G., Marin, R., Torrent, L., Ferrer, I., Diaz, M., 2011. Severe alterations in lipid composition of frontal cortex lipid rafts from Parkinson's disease and incidental Parkinson's disease. Mol. Med. 17, 1107–1118.
Farrer, M., Kachergus, J., Forno, L., Lincoln, S., Wang, D.S., Hulihan, M., Maraganore, D., Gwinn-Hardy, K., Wszolek, Z., Dickson, D., Langston, J.W., 2004. Comparison of kindreds with parkinsonism and alpha-synuclein genomic multiplications. Ann. Neurol. 55, 174–179.
Faust, M., Schuster, N., Montenarh, M., 1999. Specific binding of protein kinase CK2 catalytic subunits to tubulin. FEBS Lett. 462, 51–56.
Fortin, D.L., Troyer, M.D., Nakamura, K., Kubo, S., Anthony, M.D., Edwards, R.H., 2004. Lipid rafts mediate the synaptic localization of alpha-synuclein. J. Neurosci. 24, 6715–6723.
Fossati, G., Morini, R., Corradini, I., Antonucci, F., Trepte, P., Edry, E., Sharma, V., Papale, A., Pozzi, D., Defilippi, P., et al., 2015. Reduced SNAP-25 increases PSD-95 mobility and impairs spine morphogenesis. Cell Death Differ.
Gardoni, F., Picconi, B., Ghiglieri, V., Polli, F., Bagetta, V., Bernardi, G., Cattabeni, F., Di Luca, M., Calabresi, P., 2006. A critical interaction between NR2B and MAGUK in L-DOPA induced dyskinesia. J. Neurosci. 26, 2914–2922.
Gil, C., Falques, A., Sarro, E., Cubi, R., Blasi, J., Aguilera, J., Itarte, E., 2011. Protein kinase CK2 associates to lipid rafts and its pharmacological inhibition enhances neurotransmitter release. FEBS Lett. 585, 414–420.
Giordano, F., Saheki, Y., Idevall-Hagren, O., Colombo, S.F., Pirruccello, M., Milosevic, I., Gracheva, E.O., Bagriantsev, S.N., Borgese, N., De Camilli, P., 2013. PI(4,5)P(2)-dependent and Ca(2+)-regulated ER-PM interactions mediated by the extended synaptotagmins. Cell 153, 1494–1509.
Goebel-Goody, S.M., Davies, K.D., Alvestad Linger, R.M., Freund, R.K., Browning, M.D., 2009. Phospho-regulation of synaptic and extrasynaptic N-methyl-D-aspartate receptors in adult hippocampal slices. Neuroscience 158, 1446–1459.
Goldberg, M.S., Pisani, A., Haburcak, M., Vortherms, T.A., Kitada, T., Costa, C., Tong, Y., Martella, G., Tscherter, A., Martins, A., et al., 2005. Nigrostriatal dopaminergic deficits and hypokinesia caused by inactivation of the familial Parkinsonism-linked gene DJ-1. Neuron 45, 489–496.
Hallett, P.J., Dunah, A.W., Ravenscroft, P., Zhou, S., Bezard, E., Crossman, A.R., Brotchie, J.M., Standaert, D.G., 2005. Alterations of striatal NMDA receptor subunits associated with the development of dyskinesia in the MPTP-lesioned primate model of Parkinson's disease. Neuropharmacology 48, 503–516.
Hara, S., Arawaka, S., Sato, H., Machiya, Y., Cui, C., Sasaki, A., Koyama, S., Kato, T., 2013. Serine 129 phosphorylation of membrane-associated alpha-synuclein modulates dopamine transporter function in a G protein-coupled receptor kinase-dependent manner. Mol. Biol. Cell 24 (1649–1660), S1641–S1643.
Kornau, H.C., Schenker, L.T., Kennedy, M.B., Seeburg, P.H., 1995. Domain interaction between NMDA receptor subunits and the postsynaptic density protein PSD-95. Science 269, 1737–1740.
Laemmli, U.K., 1970. Cleavage of structural proteins during the assembly of the head of bacteriophage T4. Nature 227, 680–685.
Li, S., Jin, M., Koeglsperger, T., Shepardson, N.E., Shankar, G.M., Selkoe, D.J., 2011. Soluble Abeta oligomers inhibit long-term potentiation through a mechanism involving excessive activation of extrasynaptic NR2B-containing NMDA receptors. J. Neurosci. 31, 6627–6638.
Lieberman, D.N., Mody, I., 1999. Casein kinase-II regulates NMDA channel function in hippocampal neurons. Nat. Neurosci. 2, 125–132.
Litchfield, D.W., 2003. Protein kinase CK2: structure, regulation and role in cellular decisions of life and death. Biochem. J. 369, 1–15.
Lu, W., Man, H., Ju, W., Trimble, W.S., MacDonald, J.F., Wang, Y.T., 2001. Activation of synaptic NMDA receptors induces membrane insertion of new AMPA receptors and LTP in cultured hippocampal neurons. Neuron 29, 243–254.
Lykkebo, S., Jensen, P.H., 2002. Alpha-synuclein and presynaptic function: implications for Parkinson's disease. Neruomol. Med. 2, 115–129.
Maroteaux, L., Campanelli, J.T., Scheller, R.H., 1988. Synuclein: a neuron-specific protein localized to the nucleus and presynaptic nerve terminal. J. Neurosci. 8, 2804–2815.
Martinez, J., Moeller, I., Erdjument-Bromage, H., Tempst, P., Lauring, B., 2003. Parkinson's Disease-associated α-Synuclein Is a Calmodulin Substrate. J. Biol. Chem. 278, 17379–17387.
Melachroinou, K., Xilouri, M., Emmanouilidou, E., Masgrau, R., Papazafiri, P., Stefanis, L., Vekrellis, K., 2013. Deregulation of calcium homeostasis mediates secreted alpha-synuclein-induced neurotoxicity. Neurobiol. Aging 34, 2853–2865.
Menna, E., Zambetti, S., Morini, R., Donzelli, A., Disanza, A., Calvigioni, D., Braida, D., Nicolini, C., Orlando, M., Fossati, G., et al., 2013. Eps8 controls dendritic spine density and synaptic plasticity through its actin-capping activity. EMBO J. 32, 1730–1744.
Min, S.W., Chang, W.P., Sudhof, T.C., 2007. E-Syts, a family of membranous Ca2+-sensor proteins with multiple C2 domains. Proc. Natl. Acad. Sci. U. S. A. 104, 3823–3828.
Murphy, D.D., Rueter, S.M., Trojanowski, J.Q., Lee, V.M., 2000. Synucleins are developmentally expressed, and alpha-synuclein regulates the size of the presynaptic vesicular pool in primary hippocampal neurons. J. Neurosci. 20, 3214–3220.
Nash, J.E., Johnston, T.H., Collingridge, G.L., Garner, C.C., Brotchie, J.M., 2005. Subcellular redistribution of the synapse-associated proteins PSD-95 and SAP97 in animal models of Parkinson's disease and L-DOPA-induced dyskinesia. FASEB J. 19, 583–585.
Nikonenko, I., Boda, B., Steen, S., Knott, G., Welker, E., Muller, D., 2008. PSD-95 promotes synaptogenesis and multiinnervated spine formation through nitric oxide signaling. J. Cell Biol. 183, 1115–1127.
Perez, A.S., Bredt, D.S., 1998. The N-terminal PDZ-containing region of postsynaptic density-95 mediates association with caveolar-like lipid domains. Neurosci. Lett. 258, 121–123.
Robinson, P., Etheridge, S., Song, L., Armenise, P., Jones, O.T., Fitzgerald, E.M., 2010. Formation of N-type (Cav2.2) voltage-gated calcium channel membrane microdomains: lipid raft association and clustering. Cell Calcium 48, 183–194.
Ronzitti, G., Bucci, G., Emanuele, M., Leo, D., Sotnikova, T.D., Mus, L.V., Soubrane, C.H., Dallas, M.L., Thalhammer, A., Cingolani, L.A., et al., 2014. Exogenous alpha-synuclein decreases raft partitioning of Cav2.2 channels inducing dopamine release. J. Neurosci. 34, 10603–10615.
Rostaing, P., Weimer, R.M., Jorgensen, E.M., Triller, A., Bessereau, J.L., 2004. Preservation of immunoreactivity and fine structure of adult C. elegans tissues using high-pressure freezing. J. Histochem. Cytochem. Off. J. Histochem. Soc. 52, 1–12.
Sacino, A.N., Brooks, M., McGarvey, N.H., McKinney, A.B., Thomas, M.A., Levites, Y., Ran, Y., Golde, T.E., Giasson, B.I., 2013. Induction of CNS alpha-synuclein pathology by fibrillar and non-amyloidogenic recombinant alpha-synuclein. Acta Neuropathol. Commun. 1, 38.
Sarno, S., Reddy, H., Meggio, F., Ruzzene, M., Davies, S.P., Donella-Deana, A., Shugar, D., Pinna, L.A., 2001. Selectivity of 4,5,6,7-tetrabromobenzotriazole, an ATP site-directed inhibitor of protein kinase CK2 ('casein kinase-2'). FEBS Lett. 496, 44–48.
Scannevin, R.H., Huganir, R.L., 2000. Postsynaptic organization and regulation of excitatory synapses. Nat. Rev. Neurosci. 1, 133–141.
Simon-Sanchez, J., Schulte, C., Bras, J.M., Sharma, M., Gibbs, J.R., Berg, D., Paisan-Ruiz, C., Lichtner, P., Scholz, S.W., Hernandez, D.G., et al., 2009. Genome-wide association study reveals genetic risk underlying Parkinson's disease. Nat. Genet. 41, 1308–1312.
Singleton, A.B., Farrer, M., Johnson, J., Singleton, A., Hague, S., Kachergus, J., Hulihan, M., Peuralinna, T., Dutra, A., Nussbaum, R., et al., 2003. alpha-Synuclein locus triplication causes Parkinson's disease. Science 302, 841.
Spillantini, M.G., Schmidt, M.L., Lee, V.M., Trojanowski, J.Q., Jakes, R., Goedert, M., 1997. Alpha-synuclein in Lewy bodies. Nature 388, 839–840.
Sun, P., Wang, J., Gu, W., Cheng, W., Jin, G.Z., Friedman, E., Zheng, J., Zhen, X., 2009. PSD-95 regulates D1 dopamine receptor resensitization, but not receptor-mediated Gs-protein activation. Cell Res. 19, 612–624.
Volpicelli-Daley, L.A., Luk, K.C., Patel, T.P., Tanik, S.A., Riddle, D.M., Stieber, A., Meaney, D.F., Trojanowski, J.Q., Lee, V.M., 2011. Exogenous alpha-synuclein fibrils induce Lewy body pathology leading to synaptic dysfunction and neuron death. Neuron 72, 57–71.
Wilhelm, B.G., Mandad, S., Truckenbrodt, S., Krohnert, K., Schafer, C., Rammner, B., Koo, S.J., Classen, G.A., Krauss, M., Haucke, V., et al., 2014. Composition of isolated synaptic boutons reveals the amounts of vesicle trafficking proteins. Science 344, 1023–1028.
Winner, B., Jappelli, R., Maji, S.K., Desplats, P.A., Boyer, L., Aigner, S., Hetzer, C., Loher, T., Vilar, M., Campioni, S., et al., 2011. In vivo demonstration that alpha-synuclein oligomers are toxic. Proc. Natl. Acad. Sci. U. S. A. 108, 4194–4199.
Zenisek, D., Steyer, J.A., Almers, W., 2000. Transport, capture and exocytosis of single synaptic vesicles At active zones. Nature 406, 849–854.

Please cite this article as: Emanuele, M., et al., Exogenous Alpha-Synuclein Alters Pre- and Post-Synaptic Activity by Fragmenting Lipid Rafts, EBioMedicine (2016), http://dx.doi.org/10.1016/j.ebiom.2016.03.038